

Bitcoin’s Power Law: Weak Structure, Strong Forecasts

Carlos Baquero^{*a} and Raquel Menezes^{†b}

^aFaculty of Engineering, University of Porto and INESC TEC, Portugal

^bCentro de Matemática, Universidade do Minho, Braga, Portugal

May 21, 2026

Abstract

Bitcoin’s price has been described as following a power law (PL) in time, $P \sim t^\beta$ with $\hat{\beta} \approx 5.7$ over 2010–2026. We test this claim using the Clauset–Shalizi–Newman protocol applied to Bitcoin’s tail-relevant distributional series, and develop three principled time-domain adaptations of the protocol. We find that (i) the distributional power law is rejected on UTXO balances and daily |returns|, with lognormal preferred decisively; (ii) the fitted time-domain exponent varies by nearly a factor of three across reasonable shifts of the time origin — it is not specification-robust in the sense required for a shift-invariant structural reading; (iii) standard residual diagnostics and scale-invariance tests proposed in earlier work cannot distinguish a power law from a multi-component sigmoid stack fit to the same data; (iv) Bitcoin price stands apart in a cross-asset comparison spanning Bitcoin on-chain metrics and traditional asset classes: it is the only series in the nine-series in-sample test where no single-component growth curve improves on the power law, and the quarterly $K = 3$ wave-stability bootstrap rejects the PL+AR(1) null on Bitcoin at $p_{<15\%} = 0.015$ — a clear cross-asset separation, although not a Bonferroni-robust rejection; and (v) walk-forward Diebold–Mariano evaluation against ten candidates — including standard time-series baselines (RW with drift, auto-ARIMA, ETS, local-linear-trend) — shows the in-sample winner (multi-sigmoid) is among the worst long-horizon forecasters, while the simple power law dominates 12–24 month horizons against every standard baseline at $p < 0.05$, precisely because it does not commit to specific wave shapes. The fit–prediction tradeoff is the practical counterpart of the descriptive findings.

Keywords: Bitcoin, power law, CSN methodology, walk-forward validation, wave-stability bootstrap, adoption waves, Diebold–Mariano.

1 Introduction

Bitcoin has been continuously traded for roughly 16 years, in which time its US-dollar price has moved from cents to several tens of thousands of dollars — a span of approximately six orders of magnitude that is unusual for any traded asset. Daily prices are publicly observable, the supply schedule is fixed by protocol, and the network has accumulated a settlement history of several hundred million transactions. These features make Bitcoin a natural object of study for the kind of empirical question that econometrics rarely gets to ask of a market instrument: whether a single, well-defined functional law describes its long-run growth.

*cbm@fe.up.pt

†rmenezes@math.uminho.pt

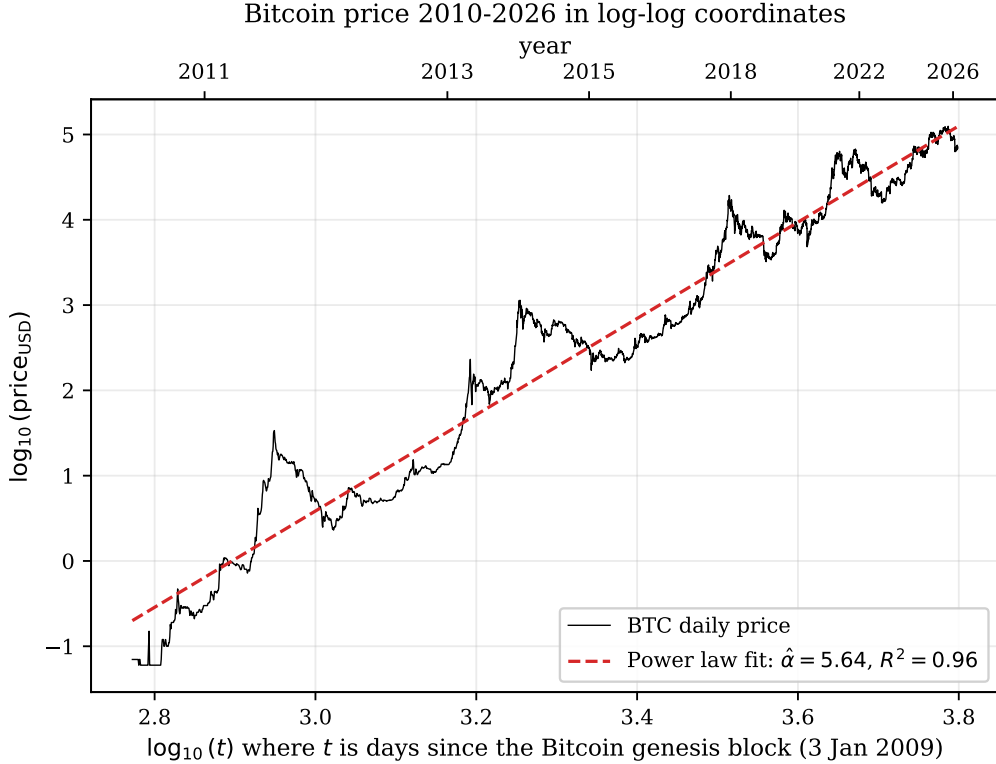


Figure 1: Bitcoin daily closing price from 18 August 2010 to 25 March 2026 ($n = 5,699$) on log–log axes. Time is days since the Bitcoin genesis block (3 January 2009); the upper axis shows calendar years for reference. The dashed red line is the power-law fit $\log_{10}(P) = \alpha \log_{10}(t) + c$ ($\hat{\alpha} = 5.64$, $R^2 = 0.96$). The data lies close to the fitted line across nearly six orders of magnitude in price.

The empirical observation that motivates such a question is shown in Figure 1: on log–log axes (price against time since Bitcoin’s genesis block in January 2009), the daily price data lies remarkably close to a straight line over the entire period 2010–2026. A straight line in log–log coordinates is the defining signature of a power law (PL) $P \sim t^\beta$, with the slope giving the exponent β . The visual fit is striking — $R^2 = 0.96$ on the OLS regression, with residual standard deviation of 0.30 in $\log_{10}(P)$ corresponding to a typical multiplicative error of about a factor of two on price.

This empirical regularity has not gone unnoticed. A power-law description of Bitcoin’s price has been proposed in successive forms over the last decade, with the most recent formal account in [Santostasi and Perrenod \(2026\)](#), who report $\hat{\beta} = 5.690$ over a comparable window and propose a mechanistic derivation in which the exponent decomposes as $\beta = \beta_A \cdot \beta_M$, with β_A describing network adoption growth and β_M a generalised Metcalfe relationship between price and network size. A related multi-component proposal by [Wheatley et al. \(2019\)](#) couples a generalised-Metcalfe value model to a Log-Periodic Power Law Singularity bubble model. The same visual log–log linearity is also used in popular discourse as the basis for long-horizon valuation projections, with central estimates that have practical consequences for portfolio allocation; the underlying empirical claim therefore deserves the same level of statistical scrutiny as any other quantitative forecast.

The temptation to take such projections at face value is not specific to Bitcoin: power-law claims of this form recur across many domains of physics, biology, and the social sciences, and they have a well-documented history of overclaiming. [Mitzenmacher \(2004\)](#) surveys the algebraic relationship between power laws and lognormal distributions and notes that visual log–log

linearity over many orders of magnitude can arise from either family, often indistinguishably. More strikingly, when the rigorous testing protocol of [Clauset et al. \(2009\)](#) is applied to large samples of empirical distributions previously labelled as power-law, only a small fraction survives: [Broido and Clauset \(2019\)](#) apply the protocol to about 1,000 real-world networks and find that 88% are fit at least as well by lognormal as by a power law.

Visual log–log linearity is therefore a necessary but not sufficient condition for a structural power law. To conclude that Bitcoin’s price–time relationship *is* a power law in the sense the term has in physics — a structural invariant of the generating process, with a well-defined and shift-invariant exponent — requires more than the OLS fit in Figure 1. [Santostasi and Perrenod \(2026\)](#) explicitly acknowledge this in their Section 11.3, noting that “the OLS estimates assume that the power law holds throughout the entire range; likelihood-ratio tests for the lower cutoff [[Clauset et al. 2009](#)] have not been applied to the temporal series.” This paper addresses that gap where the Clauset–Shalizi–Newman protocol applies directly — to Bitcoin’s tail-relevant distributional series — and develops diagnostic analogues for the time-domain regression where the canonical protocol does not mechanically apply, supplementing both with a cross-asset comparison and an out-of-sample forecasting evaluation.

Contributions. This paper makes four contributions:

1. **Distributional CSN tests.** We apply the four-step CSN protocol to Bitcoin’s tail-relevant random variables — the cross-section of UTXO balances at yearly snapshots, and the marginal distribution of daily |returns| on the full sample and three sub-periods. Eight of eleven tests reject the power-law hypothesis at $p < 0.05$, with seven of those at the bootstrap resolution limit; lognormal is preferred decisively in every case where the test has sufficient power (Section 4).
2. **Time-domain CSN adaptations.** We develop three principled adaptations of the CSN protocol for the time-domain regression $P \sim t^\beta$: a shift-parameter sensitivity sweep analogous to CSN’s x_{\min} selection; a bootstrap goodness-of-fit test on residual diagnostics; and Vuong’s likelihood-ratio test against alternative trend specifications. The first shows that the fitted exponent varies by nearly a factor of three across reasonable shifts; the second shows that standard residual diagnostics do not discriminate a power law plus realistic noise from alternative trend models; the third, supplemented by a parameter-matched flexibility check, shows that a 3-component sigmoid stack wins the in-sample comparison even against flexibility controls of equal parameter count (Section 5).
3. **Cross-series structural comparison.** We compare Bitcoin price against eight reference series — five Bitcoin on-chain metrics (hash rate, addresses, transactions, difficulty, UTXO count) and three major traditional asset classes (NASDAQ Composite, S&P 500, gold) — in an in-sample single-component comparison across all nine series (whether any of exponential, single sigmoid, quadratic, or polynomial improves on the power law), and a quarterly $K = 3$ wave-stability bootstrap on a seven-series subset (Bitcoin price, hash rate, NASDAQ, S&P 500, gold, plus Ethereum and the Global X Lithium ETF as additional candidate adoption-driven assets; the four on-chain metrics other than hash rate are omitted from the bootstrap for computational cost). *Bitcoin price is the only series in the in-sample test where no single-component specification improves on the power law, and the only series with two stable components at the strict 15%-CV threshold in the wave-stability bootstrap; it rejects the $PL+AR(1)$ null at $p_{<15\%} = 0.015$.* Two methodologically independent tests therefore converge on Bitcoin price as the distinctive series in the comparison set (Section 6).
4. **Out-of-sample forecasting evaluation.** We evaluate all candidate models, plus four standard time-series baselines (RW with drift, auto-ARIMA, ETS, local-linear-trend state-space), in walk-forward validation across 11 yearly cutoffs (2014–2024) at horizons of 1, 3,

6, 12, 18, and 24 months, with formal pairwise Diebold–Mariano significance. The multi-sigmoid that wins the in-sample comparison is among the worst at long horizons; the no-skill Naive baseline owns 1–3 month horizons; the simple power law owns 12–24 month horizons against every parametric trend specification *and* every standard time-series baseline at $p < 0.05$. The fit-prediction tradeoff is the practical counterpart of the descriptive findings (Section 8).

Roadmap. Section 2 reviews the relevant literature on power-law theory and testing, on prior Bitcoin price models, and on out-of-sample forecast evaluation. Section 3 defines the data, candidate trend specifications, evaluation metrics, and statistical tests in detail; the methodology section is deliberately self-contained and accessible to a reader with general mathematical training but no specialised background in forecasting or in power-law statistics. Sections 4–8 report the four sets of results outlined above. Section 9 synthesises the findings and distinguishes structural description from out-of-sample prediction. Section 10 summarises and identifies questions left open by this work.

2 Related work

This paper sits at the intersection of three literatures: rigorous testing of empirical power-law claims; Bitcoin price models in the time domain; and out-of-sample forecast evaluation in financial time series. We review each in turn, deliberately prioritising recent (2022–2026) work and methodological touchstones over breadth.

2.1 Power-law theory and rigorous testing

The canonical reference for empirical power-law testing is [Clauset et al. \(2009\)](#), which formalises a four-step protocol (maximum-likelihood exponent estimation with optimal lower cutoff, Kolmogorov–Smirnov bootstrap goodness-of-fit, and Vuong’s likelihood-ratio comparison against alternative distributions) and demonstrates that visual log–log linearity over many decades is not by itself sufficient evidence of a structural power law. Their framework is the methodological backbone for the distributional side of our analysis (Section 4) and the template for our time-domain adaptations (Section 5).

[Mitzenmacher \(2004\)](#) surveys the algebraic relationship between power-law and log-normal distributions, noting that small variations in generative models (preferential attachment, multiplicative processes, optimisation) produce either family and that visual discrimination over wide ranges is genuinely difficult — the motivation for using formal statistical tests rather than OLS on log–log axes. [Broido and Clauset \(2019\)](#) apply the [Clauset et al. \(2009\)](#) protocol to about 1,000 real-world networks and find that 88% are fit at least as well by lognormal as by a power law; the implied null hypothesis (“most claimed power laws fail rigorous testing”) is the methodological template for our analysis.

On the cost of confusing in-sample fit with structural truth more generally, [Bailey et al. \(2014\)](#) formalise the relationship between backtest overfitting and out-of-sample performance: they prove that under reasonable assumptions, in-sample optimisation *actively degrades* expected out-of-sample accuracy when the model-selection trial space is not disclosed. We do not engage this literature directly, but the principle motivates our parameter-matched flexibility check (Section 5.2) and our walk-forward design (Section 8).

2.2 Bitcoin price models and the time-domain power law

The most recent formal account of the Bitcoin price–time relationship is [Santostasi and Perrenod \(2026\)](#). They report $\hat{\beta} = 5.69$ over a window comparable to ours (Section 3.1), develop a

mechanistic derivation in which the exponent decomposes as $\beta = \beta_A \cdot \beta_M$ (with β_A for network adoption growth and β_M a generalised Metcalfe relationship between price and network size), and validate the empirical regularity through four scale-invariance tests — a pair-ratio test, a direct collapse test, a rolling-window stability test, and a Bayesian sequential update on local-slope estimates. Their analysis is methodologically careful within its OLS-regression framework. They explicitly acknowledge in their Section 11.3 that “likelihood-ratio tests for the lower cutoff [Clauset et al. 2009] have not been applied to the temporal series.” Our paper addresses that gap where the protocol applies directly — to Bitcoin’s tail-relevant distributions (Section 4) — and develops diagnostic analogues for the time-domain regression where it does not (Section 5), and reproduces all four of their scale-invariance tests on a synthetic 3-component sigmoid stack to characterise what those tests can and cannot demonstrate (Section 5.4).

Two related multi-component proposals frame complementary aspects of Bitcoin’s price dynamics. Wheatley et al. (2019) couple a generalised Metcalfe value model (with logistic active-user growth and exponent $\beta \approx 1.69$) to a Log-Periodic Power Law Singularity bubble model, identifying a universal super-exponential signature across four bubbles and providing ex-ante probabilistic crash brackets. Rudd and Porter (2025) propose a logistic supply-and-demand framework for Bitcoin price forecasting that explicitly substitutes a saturating diffusion process for time-only power-law extrapolation. Both are consistent with our finding that Bitcoin’s price contains multi-component saturation dynamics, though neither tests the alternative against the power law via the procedures we use.

The closest published precedent for out-of-sample rejection of a time-domain power-law specification on Bitcoin is Shelton (2024). Using the Welch–Goyal / Rapach walk-forward methodology with Campbell–Thompson R^2_{OOS} and Clark–West tests, the paper evaluates fifteen Bitcoin return predictors — including $\log(\text{time})$ — across multiple sub-periods. The $\log(\text{time})$ predictor has in-sample $R^2 = 0.002$ and OOS $R^2 = -0.070$ (worse than a no-skill mean), and the Stock-to-Flow specification of Shanaev et al. (2019) is shown to be 80.6% correlated with $\log(\text{time-since-Genesis})$ and to lose significance under time fixed effects. Our paper extends this OOS rejection from the returns to the level setting and complements it with the structural CSN tests that Shelton (2024) does not apply.

The earlier econometric critique by Shanaev et al. (2019) establishes that Bitcoin valuation regressions on hashrate and on transactions are spurious under instrumental-variable / endogeneity-corrected estimation, and that the high R^2 values typically reported in these specifications reflect common stochastic trends rather than structural relationships. We use Shanaev et al. (2019) as part of the methodological motivation for first-differencing in our causality analysis (Section 7).

2.3 Cryptocurrency forecasting and regime models

The forecasting literature on cryptocurrencies in general and Bitcoin in particular is extensive; we cite a representative sample. Catania et al. (2019) establish the methodological framework for short-horizon crypto forecasting in *International Journal of Forecasting* using dynamic model averaging and the Model Confidence Set procedure of Diebold and Mariano (1995) on 1–7 day return forecasts. Gradojevic et al. (2023) apply random forests with technical indicators to Bitcoin daily and hourly returns, finding significant outperformance of the random walk only at the daily horizon and identifying multiple structural breakpoints in predictive importance over 2015–2019. Gurgul et al. (2025) integrate transformer-based NLP, on-chain metrics, and traditional financial signals in a deep learning framework for short-horizon BTC and ETH forecasting.

For longer-horizon and regime-switching approaches more directly related to our multi-component framing, Foroutan and Lahmiri (2025) apply Bayesian MCMC covariate selection inside hidden Markov models with sixteen macroeconomic and on-chain factors over 2016–2024; they report 30-step-ahead MAPE values often exceeding 100%, providing independent

methodological corroboration of our finding that long-horizon Bitcoin point forecasts are inherently difficult. [Oprea and Bâra \(2026\)](#) train a Gaussian HMM on log-returns to infer bull/bear/sideways regimes and route each regime to a specialised forecaster, an example of regime-switching methodology applied to Bitcoin returns.

Two papers provide direct support for the no-skill-baseline half of our forecasting result. [Magner and Hardy \(2022\)](#) establish a “Meese–Rogoff puzzle” for cryptocurrencies via Wild Clark–West nested-model tests and rolling-window evaluation, finding that random-walk-with-drift baselines are difficult to beat for daily crypto returns. [Puoti et al. \(2024\)](#) use Complexity-Entropy plane and Power Spectral Density analysis to show that BTC and four other major cryptocurrencies behave like Brownian noise ($\text{PSD} \sim 1/f^2$), and that across fourteen statistical and ML forecasters the simple Naive baseline ties or beats every alternative at horizons of 1, 7, and 30 days. Their finding mirrors and corroborates our short-horizon walk-forward result (Section 8) via an independent methodological route.

Finally, [Tekin \(2024\)](#) applies Bai–Perron multiple structural-break tests to Bitcoin and Ethereum return and variance series, identifying common breakpoints aligned with COVID-era and post-pandemic shocks. The use of formal break-point econometrics on cryptocurrency series provides an empirical precedent for the structural-break methodology that our wave-stability bootstrap generalises.

2.4 Out-of-sample evaluation methodology

The methodological framework for our walk-forward forecasting evaluation rests on three foundational references. [Meese and Rogoff \(1983\)](#) establish the canonical “naive-beats-structural” result for exchange rates, showing that the random walk dominates estimated structural macro-finance models at 1–12 month horizons even when the structural models are given the unfair advantage of realised future explanatory variables. The result is one of the most replicated negative findings in empirical macroeconomics and is the natural intellectual precedent for our short-horizon Naive result on Bitcoin (Section 8). [Tashman \(2000\)](#) surveys out-of-sample evaluation practice in forecasting and codifies the walk-forward design (sequential training-set extension with origin-fixed forecast horizons) we adopt. [Diebold and Mariano \(1995\)](#) introduce the formal pairwise test for equal predictive accuracy that we use throughout Section 8; we apply the heteroscedasticity- and autocorrelation-consistent variance correction of [Newey and West \(1987\)](#) for the residual autocorrelation induced by overlapping training windows.

The statistical hazards of regressing one non-stationary series on another are formalised in [Granger and Newbold \(1974\)](#), whose spurious-regression result motivates our use of first-differencing in the causality analysis (Section 7). The augmented Dickey–Fuller stationarity tests we cite there derive from [Dickey and Fuller \(1979\)](#) and [Said and Dickey \(1984\)](#).

3 Data and methodology

This section defines the data sources, candidate trend specifications, evaluation metrics, and statistical tests used throughout the paper. The presentation is deliberately self-contained: each metric and test is introduced with intuition, formula, and interpretation guide before any empirical results appear. A specialist reader can skim; a reader with general mathematical training but no specific background in forecasting or in power-law statistics has, by the end of this section, the toolkit needed to read the rest of the paper.

Notation: α versus β . We use α for the exponent fitted in our OLS time-domain regression $\log_{10}(P) = \alpha \log_{10}(t) + c$, following standard regression-coefficient convention. Earlier work ([Santostasi and Perrenod, 2026](#); [Wheatley et al., 2019](#)) writes the same quantity as β , motivated by a generative reading of $P \sim t^\beta$. We retain β when paraphrasing those references, and the

two symbols denote the same scalar wherever they appear; the numerical values $\hat{\alpha} = 5.644$ (this paper) and $\hat{\beta} = 5.690$ (Santostasi and Perrenod, 2026) differ only because of slightly different windows (Section 3.1). One unrelated occurrence of β is the curvature parameter inside the stretched-exponential family $\log_{10}(P) = a + bt^\beta$ (Section 3.2); the context disambiguates.

3.1 Data

The primary series is the daily closing price of Bitcoin in US dollars from 18 August 2010 to 25 March 2026, $n = 5,699$ observations, obtained from the CoinDesk Bitcoin Price Index. We exclude the period before mid-2010 because exchange data is sparse and unreliable; the first publicly traded prices on liquid exchanges appear in this period. Time is measured in days since Bitcoin’s genesis block, $t_0 = 3$ January 2009. Throughout the paper, we use t to denote elapsed days since t_0 , so the first observation has $t \approx 592$ and the last $t \approx 6,291$.

We complement the price series with five on-chain metrics, daily, covering 18 August 2010 to 16 March 2026 ($n \approx 5,690$): hash rate (estimated network mining capacity), the number of unique addresses with non-zero balance, the daily count of confirmed transactions, mining difficulty, and the unspent transaction output (UTXO) count. These metrics are computed from a full archival Bitcoin node operated by the authors, with the entire blockchain processed locally; no third-party aggregator (Blockchain.com, Glassnode, Coin Metrics, etc.) is involved. This avoids any risk of inconsistencies between aggregators in how addresses are deduplicated, how UTXOs are counted at chain reorganisations, or how hash rate is estimated from block-time variance. The on-chain window aligns closely with the price window; minor end-date differences (one to two days) reflect block-time variation and have no bearing on the analyses below.

For cross-asset comparison we use daily closing prices of three benchmark assets covering the same calendar window as Bitcoin price (2010-08-18 to 2026-03-25): the NASDAQ Composite, the S&P 500, and gold (continuous front-month futures). Trading-day closures yield $n \approx 3,924$ for each benchmark — noticeably smaller than Bitcoin’s $n = 5,699$ because traditional exchanges close on weekends and public holidays, whereas Bitcoin trades continuously. Cross-asset prices are taken from Yahoo Finance.

Time from the genesis block. The genesis block is a natural absolute reference for Bitcoin: it predates any market data, is unambiguous, and matches the convention used by every prior paper that proposes a power-law relationship $P \sim t^\beta$. For cross-asset comparison we apply the same time origin: the relative positions of NASDAQ, S&P, and gold within the window are identical to Bitcoin’s, so any difference in the fitted exponents reflects the data, not the time coordinate.

Comparison with prior data windows. Our window (2010-08-18 to 2026-03-25, $n = 5,699$) is closely comparable to that used by Santostasi and Perrenod (2026) (2010-07-18 to 2026-02-18, $n = 5,696$, with an explicit exclusion of $t < 400$ days that is automatically satisfied by the data). Both windows omit pre-mid-2010 data for liquidity reasons. The slight difference at each endpoint accounts for the $\sim 0.8\%$ gap between our fitted exponent ($\hat{\alpha} = 5.644$) and theirs ($\hat{\beta} = 5.690$); we discuss this further in Section 5.

3.2 Candidate trend specifications

This subsection lists the candidate forms used for the *time-domain regression* $\log_{10}(P) = f(t) + \varepsilon$, i.e. all candidate trend models in t . These are the alternatives compared in Sections 5 and 6. A separate set of candidate *distributions* (lognormal, exponential-as-a-distribution, stretched-exponential-as-a-distribution, power law with exponential cutoff) is used in the distributional tests of Section 4; those alternatives are introduced as part of the CSN protocol in Section 3.5 (step 4).

The candidate set is organised by motivation:

- *No-skill baseline.* The naive forecast establishes the floor of forecasting skill: any model claiming predictive value must beat it, and at short horizons it is famously hard to beat for asset prices (Meese and Rogoff, 1983).
- *Power law and closely related smooth specifications.* The power law has been proposed for Bitcoin’s price–time relationship in successive forms; we adopt the most recent formalisation by Santostasi and Perrenod (2026), who report $\hat{\beta} \approx 5.69$ over a comparable window. The pure exponential is included for completeness, since it is the strict form of the casually invoked claim that “Bitcoin grows exponentially” (a claim our analysis will show holds for NASDAQ and S&P 500 over our window but not for Bitcoin). The stretched exponential is informative because its $\beta \rightarrow 0$ limit algebraically reduces to a power law, providing a natural test of smooth-model equivalence. Quadratic and cubic in t are included as generic polynomial competitors.
- *Saturation-curve alternatives.* The logistic (sigmoid) curve is the standard model for diffusion-of-innovations adoption phenomena (Bass, 1969); a stack of K sigmoids generalises this to multiple successive adoption events. Multi-component variants of this idea appear in earlier work on Bitcoin price dynamics in different forms — for example, Wheatley et al. (2019) couple a generalised-Metcalf value model (with logistic active-user growth) to a log-periodic-power-law-singularity bubble model. Our $K = 1$ case is the simplest single-saturation specification; $K = 3$ is the smallest stack that can capture multi-wave behaviour while remaining parsimonious.
- *Parameter-matched flexibility controls.* Polynomial of degree 9 (with t rescaled to $[-1, 1]$ for numerical stability) and a cubic B-spline with ten basis functions are not motivated by any specific theory; they have the same parameter count as the $K = 3$ multi-sigmoid and serve as flexibility controls. If $K = 3$ wins in-sample only because ten parameters can fit any reasonable curve, both controls should match its performance; if $K = 3$ wins because the sigmoid functional form captures structural information, the controls should fall short.
- *Standard forecasting baselines.* For out-of-sample evaluation we additionally include four baselines that are conventional in the time-series forecasting literature: random walk with drift, automatically selected ARIMA, exponential smoothing with additive trend (ETS), and a local-linear-trend unobserved-components state-space model. Unlike the trend specifications above, these baselines do not posit a deterministic parametric form for $\log_{10}(P)$ as a function of t ; they extrapolate from the recent dynamics of the level series. They are included to assess whether the power law’s long-horizon advantage in Section 8 is robust to standard time-series alternatives.

The detailed forms used throughout the paper are:

Naive (no skill):

$\hat{P}(t + h) = P(t)$. The forecast at any horizon equals the most recent observed price. Two parameters’ worth of effective information (the last value); used as the no-skill baseline for out-of-sample evaluation.

Power law (PL):

$\log_{10}(P) = \alpha \log_{10}(t) + c$. A straight line in log–log coordinates; the exponent α measures the percent change in P per percent change in t . Two parameters.

Pure exponential:

$\log_{10}(P) = at + b$. A straight line in semi-log coordinates; P doubles every fixed time interval $\ln 2/a$. Two parameters.

Quadratic and cubic in t :

$\log_{10}(P) = c + at + bt^2$ (three parameters) and the extension with a t^3 term (four parameters). Polynomial generalisations of the exponential.

Stretched exponential:

$\log_{10}(P) = a + bt^\beta$. A flexible curve that interpolates between exponential ($\beta = 1$), linear-in- t ($\beta \rightarrow 0$ in the appropriate limit), and faster-than-exponential growth. Three parameters.

Sigmoid (logistic):

$\log_{10}(P) = b + L / [1 + e^{-k(t-t_0)}]$. An S-shaped curve that grows from b to $b + L$ with maximum slope at $t = t_0$. Useful for adoption / saturation processes. Four parameters.

Multi-sigmoid stack (K components):

$\log_{10}(P) = b + \sum_{i=1}^K L_i / [1 + e^{-k_i(t-t_{0,i})}]$. A sum of K logistic curves that can capture multiple successive saturation events. We will primarily use $K = 1$ and $K = 3$. The model has $1 + 3K$ parameters; $K = 3$ has 10.

Polynomial (degree d):

$\log_{10}(P) = \sum_{j=0}^d c_j \tilde{t}^j$, where $\tilde{t} \in [-1, 1]$ is t rescaled to the training window. We take $d = 9$ (10 parameters) as a parameter-matched alternative to the $K = 3$ multi-sigmoid; the rescaling is needed for numerical stability at high degree.

Cubic B-spline (10 basis):

A piecewise cubic with knots placed at quantiles of t in the training window, expressed in the cubic B-spline basis. With ten basis functions this is also parameter-matched to $K = 3$, and provides a flexible *locally* adapting alternative.

Random walk with drift (RW-drift):

ARIMA(0, 1, 0) with constant: $\log_{10} P_t = \log_{10} P_{t-1} + \mu + u_t$ with $u_t \sim \mathcal{N}(0, \sigma^2)$. The h -step forecast is $\log_{10} P_t + h\mu$. Two parameters (μ, σ^2); the canonical baseline of asset-price forecasting (Meese and Rogoff, 1983; Magner and Hardy, 2022).

Auto-ARIMA:

ARIMA(p, d, q) with (p, d, q) selected by AIC over $p, q \in [0, 3]$, $d \in [0, 2]$ (Tashman, 2000) via the stepwise procedure of Hyndman and Khandakar (2008) as implemented in `pmдарima`.

Exponential smoothing (ETS):

Holt's linear trend $\hat{L}_t = \alpha y_t + (1 - \alpha)(\hat{L}_{t-1} + \hat{T}_{t-1})$, $\hat{T}_t = \beta(\hat{L}_t - \hat{L}_{t-1}) + (1 - \beta)\hat{T}_{t-1}$, no seasonality. Three parameters (α, β , initial level/ trend); a workhorse of practical forecasting.

Local linear trend (LLT):

Unobserved-components state-space model (Harvey and Durbin, 1986) with random level and random slope: $y_t = \mu_t + \varepsilon_t$, $\mu_t = \mu_{t-1} + \nu_{t-1} + \xi_t$, $\nu_t = \nu_{t-1} + \zeta_t$, with mutually independent Gaussian shocks. Same forecast at long horizons as a stochastic-trend extension of ETS but with explicit variance components.

3.3 In-sample evaluation metrics

We use five complementary measures to compare candidate trend specifications on the same data.

Coefficient of determination (R^2). The fraction of variance in $\log_{10}(P)$ explained by the model: $R^2 = 1 - \text{SSE}/\text{SST}$, where SSE is the sum of squared residuals and SST the total variance. Bounded between 0 and 1 and intuitive, but R^2 never decreases when parameters are added, so it cannot be used alone to compare models of different complexity.

Residual standard deviation (σ_{resid}). The typical fit error in the same units as the data: $\sigma_{\text{resid}} = \sqrt{\text{SSE}/n}$. Because we work in $\log_{10}(P)$, $\sigma_{\text{resid}} = 0.30$ corresponds to a typical multiplicative error of $10^{0.30} \approx 2$ on price.

Log-likelihood (ℓ). Under the standard assumption of Gaussian residuals, the log-likelihood of the data given the model at the maximum likelihood estimate is

$$\ell = -\frac{n}{2} [\ln(2\pi) + \ln(\hat{\sigma}^2) + 1], \quad \hat{\sigma}^2 = \text{SSE}/n.$$

Higher is better. Like R^2 , ℓ increases monotonically with flexibility; we use it as a building block, not as a model-selection criterion.

Akaike Information Criterion (AIC). $\text{AIC} = -2\ell + 2k$, where k is the number of parameters. Lower is better. AIC estimates the expected out-of-sample prediction error of a model under the Kullback–Leibler divergence to the true distribution (Akaike, 1974). As a working interpretation, differences in AIC are read on the following scale:

ΔAIC	interpretation
< 2	models essentially equivalent
2–7	clear preference for the lower-AIC model
> 10	decisive preference

Bayesian Information Criterion (BIC). $\text{BIC} = -2\ell + k \ln n$. Same form as AIC but with a heavier parameter penalty: for our n , the BIC penalty per parameter is $\ln n \approx 8.6$, more than four times the AIC penalty of 2. Lower is better. AIC is asymptotically efficient (selects the model with best prediction); BIC is consistent (selects the true model if it is in the candidate set). When the two criteria agree, the conclusion is robust to the choice of complexity penalty. We report both throughout.

Reporting multiple criteria. R^2 and σ_{resid} are intuitive descriptors but biased toward flexible models. AIC and BIC penalise complexity in different ways, and their agreement is a sensitivity check on any model selection. The log-likelihood is the underlying statistical quantity from which AIC, BIC, and the formal tests below are derived.

3.4 Vuong’s likelihood-ratio test

For two non-nested models A and B fit to the same data, Vuong’s test (Vuong, 1989) formally tests whether one provides a significantly better fit. Let $\ell_A^{(i)}$ and $\ell_B^{(i)}$ denote the pointwise log-likelihood contributions for observation i . The test statistic is

$$V = \frac{\sqrt{n} \bar{\text{LR}}}{s_{\text{LR}}}, \quad \text{LR}_i = \ell_A^{(i)} - \ell_B^{(i)}, \quad (1)$$

where $\bar{\text{LR}}$ and s_{LR} are the sample mean and standard deviation of LR_i . Under the null hypothesis that the two models are equivalent, V is asymptotically standard normal, so $|V| > 1.96$ corresponds to $p < 0.05$. A positive V means model A wins; negative means B wins.

When the two candidates have different numbers of parameters, we use the BIC-corrected variant $\bar{\text{LR}}_{\text{corrected}} = \bar{\text{LR}} + (k_A - k_B) \ln n / (2n)$, which penalises the more flexible model. This adjustment is conservative: it can only attenuate the apparent advantage of the flexible model.

Where Vuong’s test is used in this paper. The test predates the CSN protocol (Section 3.5) by two decades and is a general-purpose tool, but CSN adopted it as their fourth step. We use it in both senses, and introduce it once here to avoid re-defining it. First, as Step 4 of the canonical CSN protocol on the distributional tests of Section 4 (power law against lognormal, exponential, and stretched exponential on UTXO balances and daily |returns|). Second, in our time-domain CSN adaptation C (Section 3.6), applied directly to the time-domain regression to compare the power law against alternative trend specifications such as the multi-sigmoid stack.

3.5 The Clauset–Shalizi–Newman (CSN) protocol

Power-law claims are notoriously hard to verify by visual inspection. Log-normal, stretched-exponential, and other heavy-tailed distributions can produce convincing log–log linearity over many decades (Mitzenmacher, 2004); many published power-law claims across disciplines fail formal testing once the claim is examined rigorously (Broido and Clauset, 2019). Clauset et al. (2009) developed a four-step protocol for testing such claims that has become canonical:

1. **Estimate the lower cutoff** x_{\min} above which the power law is claimed to hold, by minimising the Kolmogorov–Smirnov (KS) distance between the fitted power law and the empirical CDF for $x \geq x_{\min}$.
2. **Estimate the exponent $\hat{\alpha}$ by maximum likelihood**, not by log–log regression. The MLE is more efficient and free of the bias of binned regression.
3. **Compute a bootstrap goodness-of-fit p-value.** Generate many synthetic datasets of size n from the fitted power law with the estimated x_{\min} ; fit a power law to each (with its own x_{\min} selection) and record the KS distance. The p-value is the fraction of synthetic KS distances \geq the observed KS distance. Values > 0.10 indicate the power law is plausible; values < 0.10 reject the power law.
4. **Compare against alternative distributions** (lognormal, exponential, stretched exponential, power law with exponential cutoff) using Vuong’s likelihood-ratio test.

The CSN protocol applies natively to *distributional* power laws — claims that some random variable X has $P(X \geq x) \sim x^{-\alpha}$. We apply it directly to two such cases for Bitcoin: the distribution of UTXO balances (yearly snapshots) and the distribution of daily |returns| (Section 4).

The time-domain claim that $P \sim t^\beta$ is a regression statement, not a distributional one. Time t is not an IID sample from some distribution but an ordered index, and the relationship asserts a deterministic trend with noise rather than the tail behaviour of a random variable. The CSN procedure cannot be applied mechanically in this setting; we develop principled adaptations next.

3.6 Time-domain CSN adaptations

We adapt three of the four CSN steps to the time-domain regression $\log_{10}(P) = \alpha \log_{10}(t+s) + c$, where $s \geq 0$ is a shift parameter (described next). Step 2 of the canonical protocol — maximum-likelihood estimation of the exponent — is not separately adapted because under Gaussian residuals OLS on the time-domain regression is itself the maximum-likelihood estimator. The remaining three steps (lower-cutoff selection, bootstrap goodness-of-fit, and likelihood-ratio comparison against alternatives) are adapted as Adaptations A, B, C below.

Diagnostic analogues, not formal CSN extensions. The canonical CSN protocol is derived for IID samples from a distribution. The time-domain regression is a different statistical object: an ordered, deterministic-trend regression with autocorrelated residuals. We therefore frame Adaptations A–C as *diagnostic analogues* rather than formal extensions: each takes a CSN-style question (does the fit depend on a free parameter? are the residuals more extreme than the null implies? does an alternative specification beat it on likelihood?) and adapts it to the time-domain setting. The diagnostics inherit the CSN protocol’s spirit — that visual fit is not enough — but their statistical guarantees are weaker than CSN’s distributional results. Specifically, the bootstrap goodness-of-fit (Adaptation B) and the wave-stability bootstrap (Section 6.2) require a model of the residual process; we use AR(1) calibrated to the data, with alternative null choices (block bootstrap, ARMA/GARCH residual models) briefly considered in Section 3.7.

The shift parameter s controls where the power-law time origin sits *relative to the genesis block*: $s = 0$ places the power-law origin at the genesis block itself, while $s > 0$ shifts the implied origin s days into the past. The shift is a methodological choice independent of when the observed data begins: our window starts at $t \approx 592$ days because Bitcoin was not liquidly traded before mid-2010, but the power-law t -coordinate is anchored to the genesis block and runs from $t = 0$ conceptually, with s controlling any offset of the fit’s reference. The default specification used throughout this paper is $s = 0$, matching [Santostasi and Perrenod \(2026\)](#); its empirical justification is given in Section 5.

Adaptation A: shift-parameter sensitivity (xmin analog). Sweep s over a grid (here, $s \in [0, 5000]$ days) and record $\hat{\alpha}(s)$, $R^2(s)$, $\text{AIC}(s)$. An exponent that is robust to specification (a necessary condition for a structural reading) should be approximately invariant to s over a reasonable range; large variation indicates that the apparent law depends on a methodological choice rather than on a property of the data alone.

Adaptation B: bootstrap goodness-of-fit on regression diagnostics. Generate B synthetic trajectories under the null that the data is generated by the fitted power law plus autocorrelated noise calibrated to the observed residuals (the noise model is described in Section 3.7). For each synthetic trajectory, compute the same residual diagnostics as on the real data (e.g., the Ljung–Box autocorrelation test ([Ljung and Box, 1978](#)), the Breusch–Pagan heteroscedasticity test ([Breusch and Pagan, 1979](#)), Chow break-test counts ([Chow, 1960](#))). The p-value is the fraction of synthetic trajectories that produce diagnostics as extreme as the observed. If the observed diagnostics fall within the synthetic distribution, the standard pathologies are non-discriminating: they are reproduced under the very null they would be used to reject.

Adaptation C: Vuong’s likelihood-ratio test against alternative trend specifications. Compare the power law against each candidate trend specification from Section 3.2 using Vuong’s test (1), with BIC correction where parameter counts differ. This is the time-domain analog of CSN step 4.

3.7 Bootstrap procedures

AR(1) noise model for time-domain bootstraps. Bitcoin’s residuals from the power-law fit are highly autocorrelated: neighbouring days’ residuals are nearly identical. We model this as a first-order autoregressive (AR(1)) process,

$$\varepsilon_t = \rho \varepsilon_{t-1} + \eta_t, \quad \eta_t \sim \mathcal{N}(0, \sigma_\eta^2),$$

with ρ and the marginal residual variance $\sigma^2 = \sigma_\eta^2 / (1 - \rho^2)$ estimated from the observed PL residuals. For Bitcoin price at $s = 0$ the calibration gives $\hat{\rho} \approx 0.998$ and $\hat{\sigma} \approx 0.302$ (reported in Section 5).

Choice of null. AR(1) is one parametric null among several plausible models for log-price residuals; alternatives include block bootstraps and ARMA/GARCH residual models that capture volatility clustering. With $\hat{\rho} = 0.998$ the AR(1) is close to the unit-root limit and inherits much of the heavy-tail and clustering behaviour of the empirical residuals through its near-random-walk persistence. We retain AR(1) as the primary specification because it is the simplest parametric form that matches the dominant autocorrelation feature of the data.

Bootstrap p-value. For any test statistic T computed on real data, we generate B synthetic trajectories under a specified null hypothesis (typically: PL plus AR(1) noise), compute T for each, and report the bootstrap p-value

$$\hat{p} = \frac{\#\{T_b^* \geq T_{\text{obs}}\}}{B}.$$

Small \hat{p} (≤ 0.05 at the conventional level) means the observed statistic is unusual under the null, and we reject the null. Bootstrap p-values are reported with “ $p < 1/B$ ” wherever the observed statistic exceeds every synthetic value.

3.8 Out-of-sample evaluation

In-sample fit quality is a measure of description, not prediction. We evaluate predictive accuracy using *walk-forward validation* (Tashman, 2000): at each of 11 yearly cutoff dates from 1 January 2014 through 1 January 2024, we fit each model on data strictly before the cutoff and forecast the price at horizons of 1, 3, 6, 12, 18, and 24 months ahead. This produces 11 forecast errors per (model, horizon) pair on $\log_{10}(P)$, with no information leakage from future to past.

Naive baseline. The naive forecast is $\hat{P}(t+h) = P(t)$ — next month’s price predicted as today’s. Because Bitcoin’s daily returns have low predictability, naive is surprisingly competitive at short horizons, as established for traditional asset classes by Meese and Rogoff (1983). Including it as a baseline gives a calibration of what “forecast skill” actually looks like.

Diebold–Mariano test. For two models A and B with squared forecast-error series $e_{A,t}^2, e_{B,t}^2$ across cutoffs, the Diebold–Mariano (DM) test (Diebold and Mariano, 1995) formally tests equal predictive accuracy. Let $d_t = e_{A,t}^2 - e_{B,t}^2$; then

$$\text{DM} = \frac{\bar{d}}{\sqrt{\widehat{\text{Var}}(d)}}, \tag{2}$$

where the variance estimate uses the heteroscedasticity- and autocorrelation-consistent (HAC) correction of Newey and West (1987). This correction is needed because forecast errors at adjacent cutoffs may be correlated — in our setting, successive training windows overlap, so a 1-year cutoff increment shares 90%+ of training data with its neighbour; without the correction the variance of \bar{d} would be underestimated and DM rejection rates inflated. We use a HAC lag of at most 2 given our 11 cutoffs. Under the null of equal accuracy, DM is asymptotically standard normal; we report two-sided p-values. With $n = 11$ cutoffs per horizon, statistical power is moderate; we therefore report effect sizes (mean RMSE differences) alongside p-values.

3.9 Causality tests

To assess the direction of information flow between Bitcoin price and each on-chain metric we use two complementary tests, both on first-differenced log series (which are stationary by the

augmented Dickey–Fuller test at $p < 0.001$ in every case). First-differencing converts growth rates into stationary changes, removing the common stochastic trend that would render levels-based regression spurious (Granger and Newbold, 1974; Shanaev et al., 2019).

Granger causality. Granger (1969) asks whether past values of X help predict Y beyond the predictive power of Y ’s own past. We test both directions (price \rightarrow metric, and metric \rightarrow price) at lag orders of 7, 14, 30, and 60 days, reporting the F-statistic and its p-value for each direction. The asymmetry ratio $F_{P \rightarrow M} / F_{M \rightarrow P}$ summarises the relative strength of the two directions: a value $\gg 1$ indicates that price changes predict metric changes more strongly than the reverse.

Cross-correlation function (CCF). The CCF measures the linear correlation between two series at varying time lags:

$$\rho_{XY}(k) = \frac{\text{Cov}(X_t, Y_{t-k})}{\sigma_X \sigma_Y}.$$

A peak at lag $k > 0$ in the CCF of (price changes, metric changes) indicates that price changes lead metric changes by k days. Where Granger reports the existence of a directional relationship, the CCF reports its time scale.

4 Distributional power-law tests

The CSN protocol (Section 3.5) was developed to test power-law claims about *random variables*, and Bitcoin offers two natural candidates for such tests: the cross-sectional distribution of unspent-transaction-output (UTXO) balances, and the marginal distribution of daily |returns|. Both are tail-relevant: in each case a power-law tail would imply a heavy-tailed phenomenon of the sort the canonical protocol was built to assess. This section applies the four CSN steps to both series, and provides a methodological baseline before we turn to the more difficult time-domain claim in Section 5.

4.1 Series tested

UTXO balance distributions. For each of seven yearly snapshots from 2013 through 2025, we extract the cross-sectional distribution of UTXO balances expressed in BTC. The number of UTXOs grows from $\sim 8 \times 10^6$ in 2013 to $\sim 3.5 \times 10^8$ in 2025, all derived from the local archival node (Section 3.1). Balances are binned into nine logarithmic buckets from $< 10^{-3}$ BTC to $> 10^3$ BTC and the CSN procedure applied to each yearly distribution.

Daily |return| distributions. Daily log-returns are $r_t = \log(P_t/P_{t-1})$. We test the distribution of $|r_t|$ on the full sample (2010-2026, $n = 5,564$ after first-differencing) and on three non-overlapping sub-periods of approximately equal length: 2010-2015 ($n = 1,828$), 2016-2020 ($n = 1,826$), and 2021-2026 ($n = 1,908$). The sub-period split lets us check whether any apparent non-power-law character of the full sample is an artefact of regime mixing: if Bitcoin’s daily |return| distribution is truly a power law within each regime but the exponent shifts across regimes, then the full sample would fail even though sub-periods would each pass.

4.2 Procedure

For each distribution we apply the four CSN steps from Section 3.5: (1) lower cutoff \hat{x}_{\min} selected by minimising the KS distance; (2) MLE exponent $\hat{\alpha}$; (3) bootstrap goodness-of-fit p using $B = 200$ synthetic samples; (4) Vuong’s likelihood-ratio test (Section 3.4) against lognormal, exponential, and stretched-exponential alternatives.

Sample-size cap. CSN’s bootstrap step requires re-fitting the power law to each synthetic sample. For the largest UTXO snapshot ($n \sim 3.5 \times 10^8$) running the bootstrap on the full sample is computationally intractable. We cap the bootstrap sample at $n = 5,000$, which is justified by two properties of the data: the binned UTXO support has only nine unique values, so re-sampling beyond that point adds no statistical information; and $n = 5,000$ is well above CSN’s conventional minimum of $n_{\text{tail}} > 50$ above the fitted cutoff.

4.3 Results

Table 1 reports the eleven tests.

Table 1: CSN distributional tests on Bitcoin’s tail-relevant series. \hat{x}_{\min} is the fitted lower cutoff; $\hat{\alpha}$ is the MLE exponent; D is the observed Kolmogorov–Smirnov distance; p is the bootstrap goodness-of-fit p-value with $B = 200$ iterations (“ < 0.005 ” indicates the resolution limit of $B = 200$). n_{tail} (in footnote) is the number of bootstrap-sample points above \hat{x}_{\min} when relevant.

Series	n	\hat{x}_{\min}	$\hat{\alpha}$	D	p	Verdict
<i>UTXO balance distributions (yearly snapshots)</i>						
2013	8.1×10^6	0.0005	1.56	0.183	< 0.005	PL rejected
2015	3.4×10^7	0.0005	1.97	0.141	< 0.005	PL rejected
2017	6.6×10^7	0.0005	1.87	0.144	< 0.005	PL rejected
2019	1.0×10^8	0.0005	2.21	0.143	< 0.005	PL rejected
2021	1.3×10^8	0.0005	2.33	0.149	< 0.005	PL rejected
2023	2.1×10^8	0.0005	2.56	0.148	< 0.005	PL rejected
2025	3.5×10^8	0.316	2.89	0.190	0.16	Plausible [†]
<i>Daily r_t distributions</i>						
Full sample 2010–2026	5,564	0.0149	2.68	0.060	< 0.005	PL rejected
2010–2015	1,828	0.0325	2.96	0.059	0.17	Plausible [†]
2016–2020	1,826	0.0171	3.00	0.086	0.035	PL rejected
2021–2026	1,908	0.0083	2.55	0.093	< 0.005	PL rejected

[†] Power-of-test artefact: tail truncation leaves the procedure underpowered. UTXO 2025: $n_{\text{tail}} = 74$ above the shifted $\hat{x}_{\min} = 0.316$. Daily 2010–2015: $n_{\text{tail}} = 234$. In both cases Vuong’s likelihood-ratio test (Section 4.4) prefers lognormal, indicating that the failure to reject reflects the test’s power, not evidence in favour of a power law.

Headline. Eight of the eleven tests reject the power-law hypothesis at $p < 0.05$, and seven of those at the $B = 200$ resolution limit of $p < 0.005$. The two “plausible” results (UTXO 2025 and daily 2010–2015) are explained by power-of-test artefacts.

The two “plausible” results.

- For UTXO 2025, \hat{x}_{\min} shifted from 0.0005 BTC (the lowest bucket, used in 2013–2023) to 0.316 BTC (the second bucket from the top), leaving only 74 effective tail observations. With so few unique values in the fitted region, the KS distance has limited power to reject. The procedure cannot find evidence against a power law when there is too little tail. This is a known limitation (Clauset et al., 2009, §3.4) and is reported alongside n_{tail} for transparency.
- For daily 2010–2015, the early Bitcoin period has very heavy-tailed returns and a small effective tail ($n_{\text{tail}} = 234$). The same procedure on 2016–2020 (similar $n_{\text{tail}} = 407$) does reject at $p = 0.035$.

Neither is evidence *for* a power law: with sufficient tail samples we always reject; the two failures-to-reject reflect truncation, not goodness of fit.

Sub-period regime mixing is not the culprit. The hypothesis that the full-sample $|\text{return}|$ distribution looks non-power-law because it averages distinct regimes is rejected within the data: 2016–2020 and 2021–2026 each individually reject at conventional levels. Only the smallest sub-period (2010–2015) fails to reject, and as noted that is a tail-truncation issue rather than evidence of a power-law fit.

4.4 Comparison against alternatives via Vuong

The bootstrap goodness-of-fit p-value reports whether the power law is plausible against itself plus noise. Vuong’s likelihood-ratio test (Section 3.4) reports whether the power law is preferred over alternative parametric distributions. The alternatives considered here are those listed as step 4 of the CSN protocol in Section 3.5: *lognormal*, *exponential*, *stretched exponential*, and *power law with exponential cutoff*. These are distributions for a random variable, distinct from the trend specifications of Section 3.2, and are the canonical alternatives in the CSN literature. Across all eleven tests, Vuong selects **lognormal** as the better fit with overwhelming evidence: R statistics range from approximately -15 on the smallest sub-period (2010-2015, where the bootstrap was underpowered) to $\sim -22,000$ on the largest UTXO snapshot, all with $p < 10^{-10}$. (Negative R indicates the second-listed model – here, lognormal – wins.) Where the bootstrap rejects PL, Vuong identifies lognormal as the better fit. Where the bootstrap is underpowered, Vuong is not, and the same lognormal preference holds.

The two procedures therefore agree, and the conclusion is robust to which test one prefers: PL is not the right family for these tail distributions; lognormal is.

4.5 Conclusion of the distributional tests

In the distributional setting — where the CSN protocol is canonical and well-established — Bitcoin’s tail-relevant series do not follow a power law. UTXO balances and daily $|\text{returns}|$ are both better described by a lognormal in every test of sufficient tail size, and the failures-to-reject are tail-truncation artefacts rather than evidence in favour of a power law.

Series selection criteria. The distributional CSN protocol applies to random variables: a cross-section of values, or the marginal distribution of an approximately stationary series. UTXO balances at a snapshot satisfy this naturally (one balance per UTXO, in a population of millions). Daily $|r_t|$ is approximately stationary after first-differencing the log-price series; the augmented Dickey–Fuller test (Dickey and Fuller, 1979; Said and Dickey, 1984) rejects a unit root at $p < 10^{-6}$ in each of the three sub-periods used below ($p = 5.9 \times 10^{-7}$, 6.9×10^{-8} , 2.4×10^{-7} for 2010-2015, 2016-2020, and 2021-2026 respectively, and $p = 1.7 \times 10^{-15}$ for the full sample). The five on-chain time series we use elsewhere in the paper (hash rate, unique addresses, transactions, difficulty, UTXO count) are scalar series with strong long-run trends, and their marginal distributions would conflate tail behaviour with growth dynamics rather than isolate any genuine power-law tail. They are therefore not candidates for the distributional test; we reserve them for the time-domain power-law tests of Section 5 and the wave-structure tests of Section 6.

This sets the methodological backdrop for what follows. The remainder of the paper turns to a separate power-law claim — that Bitcoin’s price as a function of time follows $P \sim t^\beta$. This is a regression statement rather than a distributional one (Section 3.5), and prior work that has tested it has done so via OLS rather than via CSN (Santostasi and Perrenod, 2026; Wheatley et al., 2019). The CSN methodology cannot be applied mechanically in this setting; the next section develops principled diagnostic analogues and reports their results.

5 Time-domain power-law assessment

Section 4 applied the canonical CSN protocol to Bitcoin’s tail-relevant random variables and rejected the power-law hypothesis in favour of a lognormal alternative. This section turns to a different power-law claim: that Bitcoin’s price as a function of time follows $P \sim t^\beta$. As noted in Section 3.5, this is a regression statement rather than a distributional one, so the CSN procedure does not apply mechanically. We use the three adaptations developed in Section 3.6 (shift sensitivity, bootstrap goodness-of-fit on residual diagnostics, Vuong’s likelihood-ratio test), supplement them with a parameter-matched flexibility check, and reproduce standard scale-invariance tests proposed in earlier work (Santostasi and Perrenod, 2026).

The headline of this section is that the standard tests — including those proposed in earlier work — demonstrate that Bitcoin’s price has a stable long-run average slope on log-log axes near $\hat{\alpha} \approx 5.6$, but do not by themselves identify the power law as the unique structural form generating the data. Several alternative specifications, including a multi-component sigmoid stack, are consistent with the same observations. Section 6 introduces a new test that does discriminate.

5.1 Shift-parameter sensitivity (Adaptation A)

The time-domain regression is parameterised by a shift s ,

$$\log_{10}(P) = \alpha \log_{10}(t + s) + c,$$

where $s = 0$ corresponds to the genesis block as the power-law time origin (Section 3.6). An exponent that is robust to specification should be approximately invariant to the choice of s over a reasonable range; large variation indicates that the apparent law depends on a methodological choice and so fails the most basic invariance any structural reading would require. Table 2 reports the sweep over $s \in [0, 5000]$.

Table 2: Shift-parameter sensitivity (Adaptation A). For each s we refit the time-domain regression on Bitcoin’s daily price ($n = 5,699$) and report the fitted $\hat{\alpha}$, R^2 , AIC, and residual standard deviation σ . AIC is minimised at $s = 0$.

s (days)	$\hat{\alpha}$	R^2	AIC	σ_{resid}
0	5.65	0.9595	2,528	0.302
30	5.73	0.9592	2,573	0.303
60	5.81	0.9589	2,621	0.304
120	5.97	0.9581	2,722	0.306
240	6.28	0.9565	2,939	0.313
365	6.59	0.9547	3,169	0.319
500	6.92	0.9527	3,412	0.326
1,000	8.09	0.9457	4,204	0.349
2,000	10.29	0.9342	5,294	0.385
5,000	16.49	0.9144	6,796	0.439

The fitted $\hat{\alpha}$ varies by nearly a factor of three across the range, from 5.65 at $s = 0$ to 16.49 at $s = 5,000$ (Figure 2). By AIC, $s = 0$ is the optimal specification — the AIC penalty grows monotonically with s , exceeding the AIC at $s = 5,000$ by over 4,000 units. We adopt $s = 0$ as the primary specification throughout the rest of the paper. This matches Santostasi and Perrenod (2026) and corresponds to placing the power-law time origin at the Bitcoin genesis block.

The sweep is informative beyond the choice of specification: the exponent $\hat{\alpha}$ is specification-dependent rather than specification-robust — it is a function of a free parameter s that itself must be chosen, which is the most basic invariance a structural-property reading would require.

Shift-parameter sensitivity: $\hat{\alpha}$ varies 5.65 \rightarrow 16.49 across $s \in [0, 5,000]$ days; AIC minimised at $s = 0$

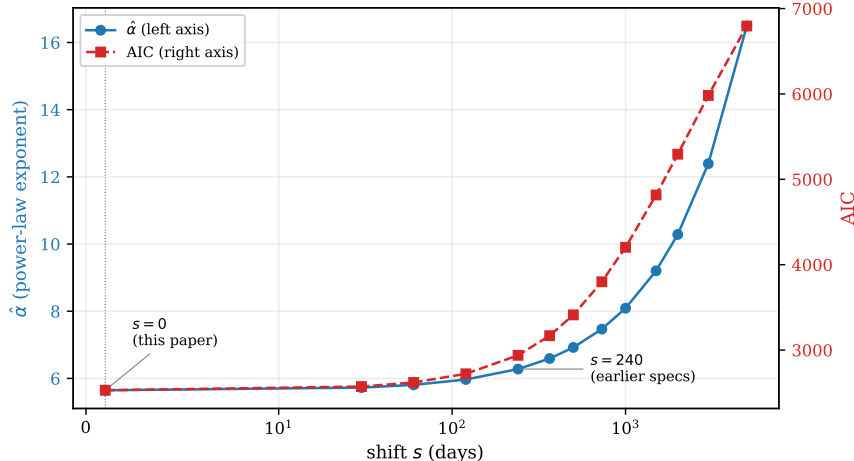


Figure 2: Shift-parameter sensitivity. Fitted power-law exponent $\hat{\alpha}$ (blue circles, left axis) and AIC (red squares, right axis) as a function of the shift s in $\log_{10}(P) = \alpha \log_{10}(t + s) + c$. Both quantities rise sharply and monotonically with s ; AIC is minimised at $s = 0$ (our specification, also matching Santostasi and Perrenod 2026). The fitted exponent varies by nearly a factor of three across the swept range, indicating that $\hat{\alpha}$ is not a shift-invariant structural property of the data.

The AIC-optimal value happens to coincide with the natural reference point (the genesis block), but using a non-zero shift of, e.g., $s = 240$ days — a value motivated in Baquero and Tinoco (2026) as a way to “reduce leverage from pre-2011 low-liquidity prices”¹ — one would report $\hat{\alpha} = 6.28$ rather than 5.65 in our coordinate. With $s = 1,000$ one would report $\hat{\alpha} = 8.09$. Differences of this magnitude across “the same data” reflect a specification-dependent exponent: there is no single shift-invariant value that the procedure recovers from the data alone.

5.2 In-sample model comparison

We compare the candidate trend specifications of Section 3.2 on the time-domain regression of Bitcoin’s daily price at $s = 0$. Table 3 reports R^2 , residual standard deviation, log-likelihood, AIC, and BIC, sorted by AIC.

Table 3: In-sample comparison of candidate trend specifications on Bitcoin’s daily price ($s = 0$, $n = 5,699$, $\log_{10}(P)$ as the dependent variable). Δ AIC is reported relative to the power law. Negative Δ AIC means the model is preferred by AIC.

Model	params	R^2	σ	log-lik	AIC	BIC	Δ AIC
Multi-sigmoid (K=3)	10	0.9742	0.241	+19.3	-19	48	-2,547
Polynomial (deg 9)	10	0.9658	0.278	-783.7	1,587	1,654	-941
Cubic B-spline (10)	10	0.9648	0.282	-864.5	1,749	1,815	-779
Power law	2	0.9595	0.302	-1,262	2,528	2,541	0
Stretched exponential	3	0.9595	0.302	-1,262	2,530	2,550	+2
Cubic	4	0.9559	0.315	-1,509	3,025	3,052	+497
Sigmoid (K=1)	4	0.9522	0.328	-1,739	3,485	3,512	+957
Quadratic	3	0.9474	0.344	-2,009	4,023	4,043	+1,495
Pure exponential	2	0.8738	0.533	-4,502	9,008	9,021	+6,480

¹Their formulation places s relative to days-since-first-observation rather than days-since-genesis, so the numerical equivalence is approximate; the qualitative point that earlier work used non-zero shifts holds.

Four observations follow.

1. Smooth alternatives collapse to the power law. The stretched exponential ranks alongside the power law: identical R^2 to four decimal places, identical σ , and a ΔAIC of exactly +2 (the parameter penalty for the unused β). The optimiser drives the stretched-exponential’s β parameter to $\sim 10^{-6}$, in which limit $t^\beta = e^{\beta \ln t} \approx 1 + \beta \ln t$, and the model algebraically reduces to a power law in $\ln t$ with effective exponent $b\beta$. Computing $b\beta \cdot \ln 10$ recovers the directly-fitted $\hat{\alpha} = 5.644$ to five decimal places. This collapse, observed informally in an earlier public discussion,² indicates that the *smooth-trend class* in our candidate set is essentially equivalent to the power law on this data.

2. The pure exponential is decisively rejected. $\Delta\text{AIC} = +6,480$ relative to the power law. Bitcoin does not grow exponentially over our window; the casual “exponential growth” framing is inconsistent with the data.

3. The multi-sigmoid stack ($K = 3$) wins by a substantial margin in-sample. $\Delta\text{AIC} = -2,547$; Vuong’s BIC-corrected likelihood-ratio test (Section 3.4) gives $V = -19.74$, $p < 10^{-80}$. The result is robust to the choice of complexity penalty: BIC, which penalises the multi-sigmoid’s eight extra parameters more heavily than AIC, also prefers $K = 3$ over the power law by $\Delta\text{BIC} = 48 - 2,541 = -2,493$. Notably, the single sigmoid ($K = 1$) is substantially worse than the power law ($\Delta\text{AIC} = +957$, $\Delta\text{BIC} = +971$), so the in-sample improvement of $K = 3$ comes from the multi-component structure, not from a single saturation event.

4. Parameter-matched flexibility check. Two flexible alternatives — polynomial of degree 9 (10 parameters, in normalised t) and cubic B-spline with 10 basis functions — match $K = 3$ in parameter count. Both improve over the power law substantially ($\Delta\text{AIC} = -941$ and -779 respectively), but $K = 3$ still wins by an additional 1,605 and 1,767 AIC units beyond the flexibility budget. This indicates that the in-sample advantage of $K = 3$ is not driven solely by having more parameters: the sigmoid functional form contributes beyond raw flexibility.

Caveat: AIC is not a sufficient structural test. The raw ΔAIC of $-2,547$ for $K = 3$ vs the power law overstates the structural evidence. As a control, we generated a synthetic dataset of the same length under the null that the data is a true power law plus AR(1) noise (with ρ and σ calibrated to Bitcoin’s residuals); the same comparison on this synthetic gives $\Delta\text{AIC} = -4,552$ for $K = 3$ vs PL — larger in magnitude than what we observe on real Bitcoin. Strong AR(1) noise produces slow-varying residual patterns that the multi-sigmoid’s flexibility can absorb, inflating the AIC advantage of the more flexible model regardless of the underlying generative process. AIC alone therefore cannot distinguish a true power-law generator from a multi-component generator on data of this length and autocorrelation. For our in-sample structural evidence, we rely on the parameter-matched flexibility check (point 4 above), which is unaffected by this caveat: all three ten-parameter alternatives (multi-sigmoid, polynomial, B-spline) share the same parameter budget, so the AIC gap among them isolates the contribution of functional form.

5.3 Bootstrap goodness-of-fit on residual diagnostics (Adaptation B)

The power-law residuals on real Bitcoin price exhibit several pathologies at conventional significance levels. We use five standard residual tests, each defined briefly here for the reader who has not seen them before. In each test the null hypothesis is that residuals behave as expected

²<https://x.com/Giovann35084111/status/2049786216988737700>

under a well-specified regression with independent, identically distributed Gaussian noise; a small p-value rejects the null and indicates a specific form of misspecification.

- *Ljung–Box test* ([Ljung and Box, 1978](#)). Tests whether residuals at lags $1, 2, \dots, h$ are jointly uncorrelated. Rejection indicates serial autocorrelation. On real BTC at $h = 50$, the test statistic is $\sim 2.4 \times 10^5$ with $p \approx 0$.
- *Breusch–Pagan test* ([Breusch and Pagan, 1979](#)). Tests whether residual variance depends on the regressors. Rejection indicates heteroscedasticity. On real BTC the LM statistic is ~ 822 with $p < 10^{-180}$.
- *Shapiro–Wilk test* ([Shapiro and Wilk, 1965](#)). Tests whether residuals are normally distributed; rejection indicates non-normality. On a 5,000-point subsample of BTC residuals (the maximum sample the test handles tractably), $p < 10^{-40}$.
- *Jarque–Bera test* ([Jarque and Bera, 1980](#)). A second normality test based on skewness and excess kurtosis of the residuals. On real BTC the statistic is ~ 693 , $p < 10^{-150}$, with skewness 0.83 and excess kurtosis 0.41.
- *Chow break test* ([Chow, 1960](#)). Tests whether the regression coefficients are stable across a candidate breakpoint; rejection indicates a structural break. On real BTC the test is applied at six biennial candidate dates from 2013 to 2023; all six reject at conventional significance.

These rejections are conventional in the sense that the residuals are clearly not the well-behaved Gaussian white noise of a correctly specified regression. Adaptation B asks whether they are *discriminating*: would they distinguish a power law plus realistic noise from data generated by some alternative process?

We generate $B = 100$ synthetic trajectories under the null that the data is generated by the fitted power law plus AR(1) noise (Section 3.7; calibrated $\hat{\rho} = 0.998$, $\hat{\sigma} = 0.302$). For each synthetic trajectory we compute the same residual diagnostics. The bootstrap p-value is the fraction of synthetic trajectories whose diagnostic value matches or exceeds the observed.

The result is uncomfortable but informative: across all five diagnostics, the synthetic distribution either matches or exceeds the observed values. Bootstrap p-values exceed 0.50 for each diagnostic; in over half of the synthetic trajectories generated from a true power law plus realistic noise, the residuals show “pathology” of the same magnitude as observed on real Bitcoin.

The conclusion is methodologically important: standard residual diagnostics, applied to a power-law regression on a series with the autocorrelation structure of Bitcoin’s price, are not informative for distinguishing PL plus noise from alternative trend models. They reject the null of well-behaved residuals, but they do so equally on data that genuinely is a power law plus realistic noise. Such diagnostics cannot serve as evidence against the power-law specification — a lesson that applies to any test of power-law claims on heavily autocorrelated time series.

5.4 Reproduction of scale-invariance tests

A separate line of argument for the power-law specification rests on tests of scale invariance — properties of the price–time relationship that should be preserved if the underlying process is truly $P \sim t^\beta$. Earlier work ([Santostasi and Perrenod, 2026](#)) proposes four such tests on Bitcoin’s price: a pair-ratio test, a direct collapse test, a rolling-window stability test, and a Bayesian sequential update on local-slope estimates. We reproduce all four on Bitcoin’s price series and on a synthetic comparison trajectory: a 3-component sigmoid stack fit to the same prices, evaluated at the same time points.

The rationale for the synthetic comparison is that scale-invariance tests are typically motivated by the question “does the data behave like a power law?” — a binary check against an

unspecified alternative. The 3-sigmoid synthetic, fit to match the actual price trajectory, has the same long-run average slope by construction; if the tests cannot distinguish it from the real data, they are passing on a property that does not identify the power law specifically.

Pair-ratio test. For 4,000 random pairs of time points (t_1, t_2) with $t_2 > t_1$, compute $\log_{10}(P(t_2)/P(t_1))$ and plot against $\log_{10}(t_2/t_1)$. A power law $P(t) = At^\beta$ produces a straight line with slope β . We replicate the test on real Bitcoin and on the sigmoid synthetic.

	Real BTC	3-sigmoid synthetic
Binned slope	5.69	5.74
R^2	0.998	0.999
Quadratic curvature	0.42	0.33

Both produce essentially perfect linearity with closely matched slopes. The synthetic actually outperforms real Bitcoin slightly (higher R^2 , smaller curvature), since it has no noise. The test does not distinguish.

Direct collapse test. Find the exponent β^* that makes the residual mean of $\log_{10}(P(\lambda t)/P(t)) - \beta \log_{10} \lambda$ flat as a function of $\log_{10} \lambda$ for $\lambda \in [1.1, 5.0]$. Under a true power law, $\beta^* = \beta$.

	Real BTC	3-sigmoid synthetic
OLS β	5.62	5.65
Collapse β^*	5.60	5.64

Both yield consistent β^* values that match their direct OLS estimates. The test does not distinguish.

Rolling temporal stability. A rolling-window estimate $\beta^*(t)$ should be stationary if the underlying generative process is a stable power law. We compute rolling estimates over 145 windows.

	Real BTC	3-sigmoid synthetic
Median β^*	5.74	5.79
Std β^*	0.48	0.37
Drift slope (per day)	1.7×10^{-5} ($p = 0.49$)	2.3×10^{-5} ($p = 0.23$)
% above median	62%	74%

Neither shows significant secular drift; both are quasi-stationary with similar median and amplitude. The test does not distinguish.

Bayesian sequential update. A conjugate Gaussian update on local $\hat{\beta}$ estimates should shrink the posterior precision τ_n as $\sigma_{\text{emp}}/\sqrt{n}$ if the underlying parameter is constant. We compute this for both datasets, with the prior calibrated separately to each dataset’s empirical local-estimate variance. The resulting $\tau_n/(\sigma_{\text{emp}}/\sqrt{n})$ is essentially 1 in both cases (real BTC: 0.999 ± 0.001 ; synthetic: 1.000 ± 0.001 , across the full sequence). Both datasets exhibit textbook $1/\sqrt{n}$ shrinkage of the posterior precision. The test does not distinguish.

What the four tests collectively demonstrate. The four scale-invariance tests confirm that Bitcoin’s price has a stable long-run average slope near $\hat{\alpha} \approx 5.6$ over the observation window. This is a real and remarkable empirical regularity. But the tests are constructed to detect departures from a stable average slope; they pass as soon as such an average exists, regardless of whether the underlying generative process is a true power law or a multi-component model whose envelope matches. The 3-sigmoid synthetic, fit to match Bitcoin’s trajectory, has the same long-run average slope by construction, and consequently passes the same tests. The tests are necessary but not sufficient for a structural power-law claim.

5.5 Conclusion of the time-domain assessment

Four results from this section can be summarised as follows.

- The power-law exponent $\hat{\alpha}$ depends on the shift parameter s , varying by nearly a factor of three across the range $s \in [0, 5,000]$. The fitted exponent is specification-dependent rather than specification-robust — it is not a shift-invariant property of the data alone.
- The multi-sigmoid stack ($K = 3$) wins the in-sample comparison decisively in AIC and Vuong’s likelihood-ratio test. The win persists at parameter-matched count against polynomial and B-spline alternatives, indicating that the sigmoid functional form contributes beyond raw flexibility, although the raw AIC advantage is partially inflated by AR(1) noise.
- Standard residual diagnostics on the power-law fit reject at conventional levels, but they reject equally on synthetic data generated as a true power law plus realistic noise. They are not discriminating.
- Scale-invariance tests proposed in earlier work pass on real Bitcoin, but they also pass on a 3-sigmoid synthetic fit to the same data. They demonstrate the long-run average slope is stable, which is real, but they do not by themselves identify the power law as the unique structural form.

These results establish two things. First, in the canonical sense required for a structural reading — a fitted exponent invariant to the basic specification choices — Bitcoin’s price-time relationship fails the test: the exponent depends on the shift parameter, and the standard residual and scale-invariance tests cannot distinguish a power law from a multi-component alternative on this data. Second, the in-sample data contains genuine information that prefers the multi-component alternative, but the standard distributional and scale-invariance tests cannot extract it. What the data actually says about Bitcoin’s price structure — and how to test it rigorously — is the subject of the next section.

6 Wave structure: a Bitcoin-specific finding

Section 5 established that the standard tests of structural form — CSN adaptations and the scale-invariance tests proposed in earlier work — cannot distinguish a power law from alternative trend specifications on Bitcoin’s price. The data contains genuine information that prefers a multi-component description, but the standard tests do not extract it.

This section introduces a test that does discriminate, using cross-series comparison: the in-sample functional-form comparison runs across nine series (Bitcoin price, five Bitcoin on-chain metrics, and three major traditional asset classes); the quarterly $K = 3$ wave-stability bootstrap runs on a seven-series subset (Bitcoin price, hash rate, NASDAQ, S&P 500, gold, plus Ethereum and a lithium ETF as additional candidate adoption-driven assets). Bitcoin price is the only series in the in-sample test where no single-component growth model improves on the power law. In the wave-stability bootstrap, Bitcoin price rejects the PL+AR(1) null at $p_{<15\%} = 0.015$;

the other six series sit in the null (Ethereum is the second-closest to rejection at $p_{<25\%} = 0.030$, the rest comfortably above conventional thresholds).

6.1 Functional form: $K = 1$ sigmoid versus power law across nine series

We applied the in-sample model comparison from Section 5.2 to nine series, all over the same calendar window 2010-08-18 to 2026-03-25 (the on-chain series end one to two days earlier, at 2026-03-16). For each series we fit the candidates of Section 3.2 and recorded the AIC difference relative to the power law. Table 4 focuses on the comparison most relevant to identifying Bitcoin price’s distinctive behaviour: the single-sigmoid ($K=1$) specification against the power law.

Table 4: Single-component model comparison across nine series. For each series we report the ΔAIC of the $K=1$ sigmoid and of the pure exponential, both relative to the power law on the same series. Negative values indicate the alternative is preferred to the power law. **Bitcoin price is the only series in the sample where the $K=1$ sigmoid does not improve on the power law**, and the only series where neither single-component alternative ($K=1$ sigmoid or pure exponential) wins.

Series	ΔAIC : $K=1$ vs PL	ΔAIC : Pure exp vs PL	$K=1$ wins?
Bitcoin price	+957	+6,480	No (PL wins)
Bitcoin hash rate	-4,781	+8,784	Yes
Bitcoin unique addresses	-9,123	+4,908	Yes
Bitcoin transactions	-6,022	+5,055	Yes
Bitcoin difficulty	-4,797	+8,845	Yes
Bitcoin UTXO count	-5,164	+7,617	Yes
NASDAQ Composite	-5,265	-5,263	Yes ($\approx exp$)
S&P 500	-5,706	-5,768	Yes ($\approx exp$)
Gold (continuous front-month)	-6,198	-1,340	Yes

Three regimes visible across the nine series. The same $K=1$ specification behaves differently across the nine series, and the pattern is informative.

For **NASDAQ and S&P 500**, the $K=1$ sigmoid and the pure exponential perform almost identically (within 60 AIC units of each other), and both beat the power law by $\sim 5,000$ - $6,000$ AIC units. Mathematically this is expected: for t well below a sigmoid’s inflection point, $\log_{10}(P) = b + L/(1 + e^{-k(t-t_0)})$ is approximately linear in t , so the sigmoid *degenerates* to a pure exponential. For these two indices the saturation point t_0 falls past 2026, and the observed window lies entirely in the early-exponential phase of any fitted single sigmoid. Both specifications therefore describe the same empirical fact: NASDAQ and S&P 500 grew approximately exponentially over our window.

For **gold**, the $K=1$ sigmoid wins by 4,858 more AIC units than the pure exponential. Gold has visible within-window dynamics that an exponential cannot capture (a rise to $\sim \$1,900$ in 2011, plateau and decline through 2018, rise again 2019+). The sigmoid’s saturation curve fits this; the exponential cannot.

For **the five Bitcoin on-chain metrics**, the $K=1$ sigmoid beats the power law by 4,800-9,100 AIC units, and decisively beats the pure exponential. The on-chain series are well described as smooth saturation curves — adoption-curve shapes consistent with the diffusion-of-innovations literature (Bass, 1969, also Section 3.2).

For **Bitcoin price**, neither specification works: $\Delta\text{AIC} = +957$ for $K=1$ vs the power law, and +6,480 for pure exponential. **It is the only series in our nine-series sample where no single growth component — whether exponential, saturating, or otherwise — improves on the power law.** The multi-component $K=3$ specification, in contrast, beats the

Cross-series in-sample fit (Δ AIC vs power law). Bitcoin price is the only row where $K=1$ sigmoid loses to PL.

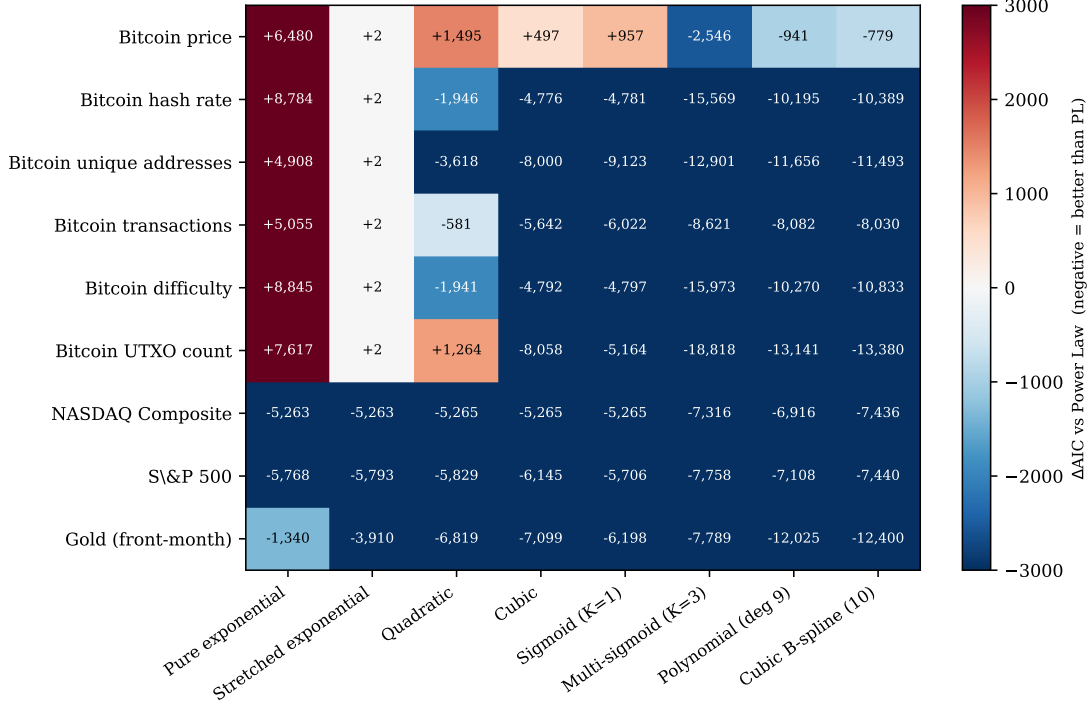


Figure 3: Cross-series in-sample fit comparison. For each of the nine series (rows) and each of the eight non-power-law candidates (columns), the cell shows Δ AIC vs the power-law fit on the same series. Negative (blue) values mean the candidate beats the power law; positive (red) values mean the power law wins. Bitcoin price (top row) is the only row where both single-component candidates — the $K=1$ sigmoid and the pure exponential — have positive Δ AIC. Stretched exponential collapses to the power law on every series (Δ AIC = +2 exactly, the parameter-penalty cost of the unused β).

power law on Bitcoin price by 2,547 AIC units (Table 3). The result holds at parameter-matched count (Section 5.2, observation 4).

The $K=1$ -versus-PL asymmetry is therefore not a result internal to Bitcoin’s on-chain ecosystem, nor a feature of the comparison methodology. It is a property specific to Bitcoin price, and not to any of the eight other series tested.

Figure 3 shows the full Δ AIC pattern across all eight non-power-law candidates and all nine series. The Bitcoin price row is the only row in which the $K = 1$ and Pure exponential cells are positive (worse than power law); every other series has at least one single-component model that improves on the power law.

6.2 The $K = 3$ wave-stability bootstrap

The single-component-fails finding suggests Bitcoin price has multi-component structure. The $K=3$ wave-stability bootstrap formalises this and tests it against the null hypothesis that the data is a power law plus realistic noise.

The test. The $K=3$ multi-sigmoid (Figure 4, top panel) is fit at 41 quarterly cutoff dates (2016-Q1 through 2026-Q1); for each cutoff we record the amplitude L_i of each of the three component sigmoids. A component is classified as *stable* if its amplitude has coefficient of

variation $CV < 25\%$ across the 41 cutoffs.³ We count the number of stable components on the real data.

Amplitude as the test statistic. Each fitted sigmoid component has three parameters — amplitude L_i , slope k_i , and inflection date $t_{0,i}$ — and any of them could in principle anchor a stability test. We choose amplitude for four reasons. First, $CV = \sigma/\mu$ is dimensionless, so a single threshold (25%, 15%) applies uniformly across series whose amplitudes differ by orders of magnitude. Inflection dates are measured in days, and a “stable” threshold for them would require ad-hoc normalisation relative to the training window. Second, amplitude has direct interpretation as the persistent log-price gain attributable to a wave; inflection dates depend on the phase of the wave and are less interpretable when the wave is still in progress. Third, amplitudes are bounded below by construction ($L \geq 0$), while inflection dates can saturate at the boundary of the training window in early cutoffs and produce noisy variance estimates. Fourth, under the PL+AR(1) null, L wanders unboundedly across spurious $K=3$ fits, whereas t_0 is constrained to lie inside the data range; the wider null distribution on L gives the test more discrimination power against a stably-identified real wave.

Choice of $K = 3$. The multi-sigmoid family (Section 3.2) admits any positive integer K ; the choice of $K = 3$ is motivated as the smallest stack that contains the wave count visible in Bitcoin’s price history over our window: two clearly completed cycles (2011-2013, 2015-2017) and one in progress (2020-2024). Smaller K would force the fit to merge cycles; larger K would introduce components for hypothetical waves not yet observed and could not be stably identified. A $K = 4$ or $K = 5$ stability bootstrap would test whether additional waves are statistically detectable, and is a natural extension of the test below; we do not pursue it here.

If Bitcoin price has genuine multi-component structure, the $K=3$ fits at successive cutoffs should consistently identify the same underlying components, and at least some component amplitudes should be stable across cutoffs. If Bitcoin price is just a power law with autocorrelated noise, the $K=3$ fit will overfit different patterns at different cutoffs, and component amplitudes will be unstable.

To test, we generate $B = 200$ synthetic trajectories under the null that the data is a power law plus AR(1) noise (calibrated $\hat{\rho} = 0.998$, $\hat{\sigma} = 0.302$, matching Bitcoin’s own residuals — Section 3.7). For each synthetic trajectory we re-run the $K=3$ fits at the same 41 cutoffs and count stable components. The bootstrap p-value is the fraction of synthetic trajectories that produce at least as many stable components as the real data.

Conservatism of the test. A negative-control simulation, in which the synthetic generator is instead a true 3-sigmoid stack plus the same AR(1) noise, yields a wave-stability bootstrap p-value of approximately 0.50 in our calibration. The test is biased toward null results: even on data that genuinely has 3-component structure, the bootstrap often fails to detect it. Reasons include: at early cutoffs (e.g., 2016) the $K=3$ fit must accommodate three sigmoids over only one or two empirically-visible waves, producing variable component parameters by construction. We mention this here because it means *small* p-values from this test are conservative indicators of true wave structure, not anti-conservative.

Result for Bitcoin price. We adopt quarterly cutoffs ($N = 41$ from 2016-Q1 through 2026-Q1) as the primary resolution: this is the coarsest schedule for which the per-component CV estimator has acceptable variance, and the finest schedule for which adjacent cutoffs share

³We also report the stricter threshold $CV < 15\%$. The 25% threshold is permissive enough that a marginally identifiable wave can clear it; the 15% threshold demands very tight stability.

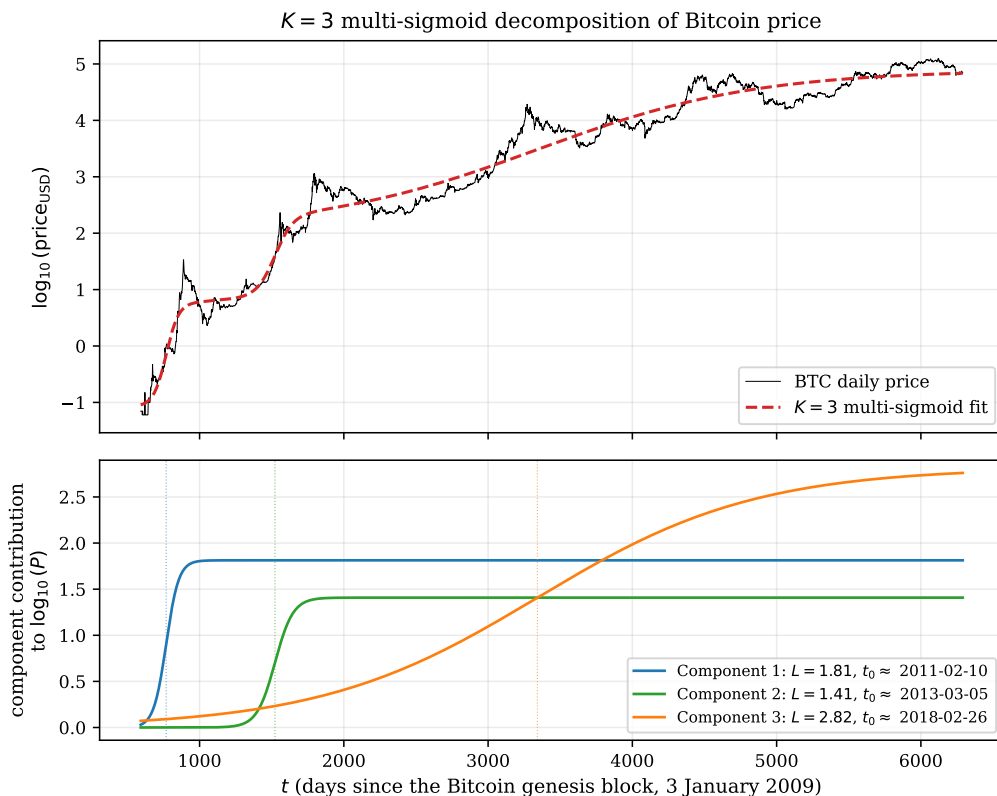


Figure 4: Top: Bitcoin daily price (black) and the multi-sigmoid ($K = 3$) fit on the full sample (red dashed). Bottom: the three fitted sigmoid components individually, sorted by inflection date. Each component contributes a saturating S-curve; their sum plus a baseline equals the top-panel fit. Inflection dates t_0 are labeled at the foot of each sigmoid for reference. The wave-stability bootstrap of Section 6.2 tests whether the amplitudes L of these three components are identifiable consistently when the same $K = 3$ fit is repeated at successive rolling cutoffs.

meaningfully new training data.⁴ Real Bitcoin price produces 2 stable components at the strict 15% CV threshold and 2 stable components at the 25% threshold. Of 200 synthetic PL+AR(1) trajectories, 3 produce ≥ 2 stable components at 15% and 13 at 25%, giving the bootstrap p-values $p_{<15\%} = 0.015$ and $p_{<25\%} = 0.065$ (Figure 5, left panel).

Corroboration from inflection-date stability. As a corroborating check, we also record the standard deviation of each component’s inflection date $t_{0,i}$ across the 41 cutoffs. On real Bitcoin price these are [19, 149, 505] days for waves 1, 2, 3 respectively: the first wave’s inflection is pinned to within ~ 19 days across a decade of rolling cutoffs, the second to within five months, while the third (the 2020–24 cycle, still in progress at the end of our window) has a much wider posterior. The pattern matches the amplitude-CV ranking (7.2%, 14.1%, 36.0%): the same two waves identified as amplitude-stable also have tightly identified inflection dates. We report this as a supplementary check rather than as a primary test, for the reasons given above (no natural threshold; boundary effects at early cutoffs); the numerical values are saved in the bootstrap JSON outputs.

The single-panel parallel-coordinates view in Figure 6 shows all 200 synthetic realizations of the per-wave CV vector against the real-data realization, making the per-component discrimi-

⁴A lower-resolution yearly schedule ($N = 11$) gives directionally consistent results with weaker statistical power ($p_{<15\%}^{\text{yearly}} = 0.190$, $p_{<25\%}^{\text{yearly}} = 0.055$); the strengthening at the strict threshold under the quarterly schedule reflects the more accurate per-component CV estimate at higher N .

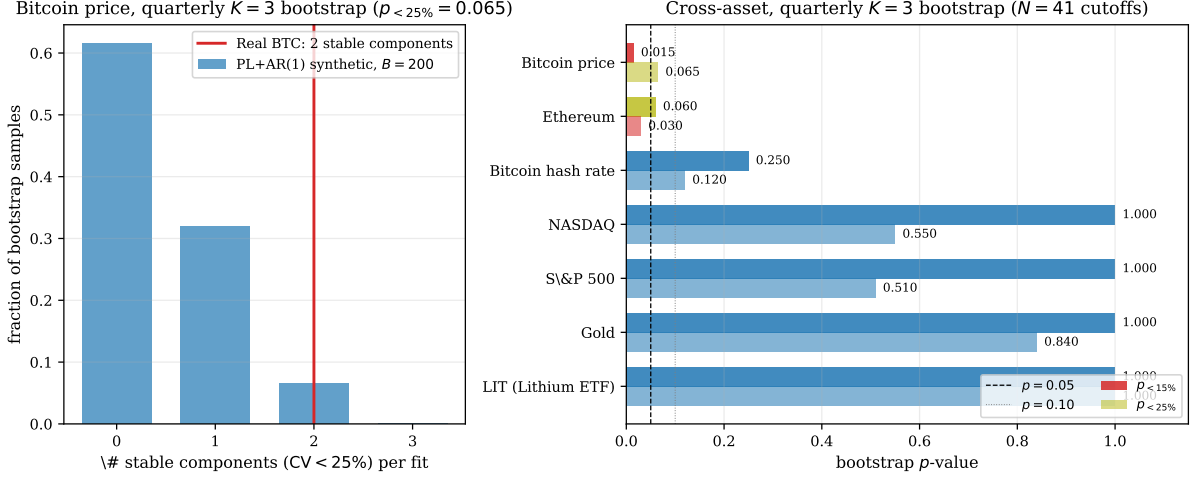


Figure 5: Quarterly $K = 3$ wave-stability bootstrap. Left: the bootstrap distribution for Bitcoin price. Bars give the fraction of $B = 200$ synthetic PL+AR(1) trajectories producing 0, 1, 2, or 3 stable components at the loose $CV < 25\%$ threshold. The vertical red line marks the real Bitcoin observation (2 stable components); only $13/200 = 6.5\%$ of synthetic trajectories produce as many or more, giving the bootstrap $p_{<25\%} = 0.065$. The corresponding strict-threshold test gives $p_{<15\%} = 0.015$ (Bitcoin row of the right panel). Right: bootstrap p -values for the same quarterly test applied to the seven-series cross-asset comparison (Table 5); both the strict (15%) and loose (25%) thresholds are reported per series. Red bars are below $p = 0.05$; tan bars are between 0.05 and 0.10; blue bars are above 0.10. Bitcoin and Ethereum are the only two series with any p -value below 0.05.

nation visible:

Interpretation. At quarterly resolution, the strict-threshold result rejects the PL+AR(1) null at conventional significance ($p_{<15\%} = 0.015$); the loose-threshold result is marginal ($p_{<25\%} = 0.065$, just above 0.05 and detectable at the 10% level). Both readings put Bitcoin in tension with the PL+AR(1) null. The result is subject to the conservatism caveat (the test is biased toward null; on a true 3-sigmoid generator it returns $p \approx 0.50$), and to the cross-asset Bonferroni correction (Section 6.3) which further tempers the single-series interpretation; we discuss both in Section 6.3.

6.3 Cross-asset corroboration

The wave-stability bootstrap was applied at quarterly cutoff resolution ($N = 41$ cutoffs from 2016-Q1 through 2026-Q1) to a seven-series comparison set organised in three groups:

- *Bitcoin ecosystem*: Bitcoin price (the focal series, $B = 200$) and hash rate ($B = 100$).⁵
- *Other adoption-driven asset candidates*: Ethereum (daily price-USD series from the Coin-Metrics community API, $n = 3,883$ days, 2015-08 to 2026-03) and the Global X Lithium & Battery Tech ETF (LIT, $n = 3,942$ days, 2010-07 to 2026-03), included as a test of whether wave structure is Bitcoin-specific or shared across other assets whose price dynamics are plausibly driven by discrete cohort-by-cohort adoption.

⁵The remaining four on-chain metrics from the in-sample comparison (unique addresses, transactions, difficulty, UTXO count) were omitted from the quarterly bootstrap: their in-sample $K = 1$ -vs-PL profiles closely resemble that of hash rate (Table 4), and each iteration of the $K=3$ fit on these series is substantially slower than on price. Unique addresses was run at the coarser yearly resolution ($N = 11$, $B = 100$, $p_{<25\%} = 0.67$) to confirm the null reading; the remaining three were not bootstrapped at either resolution.

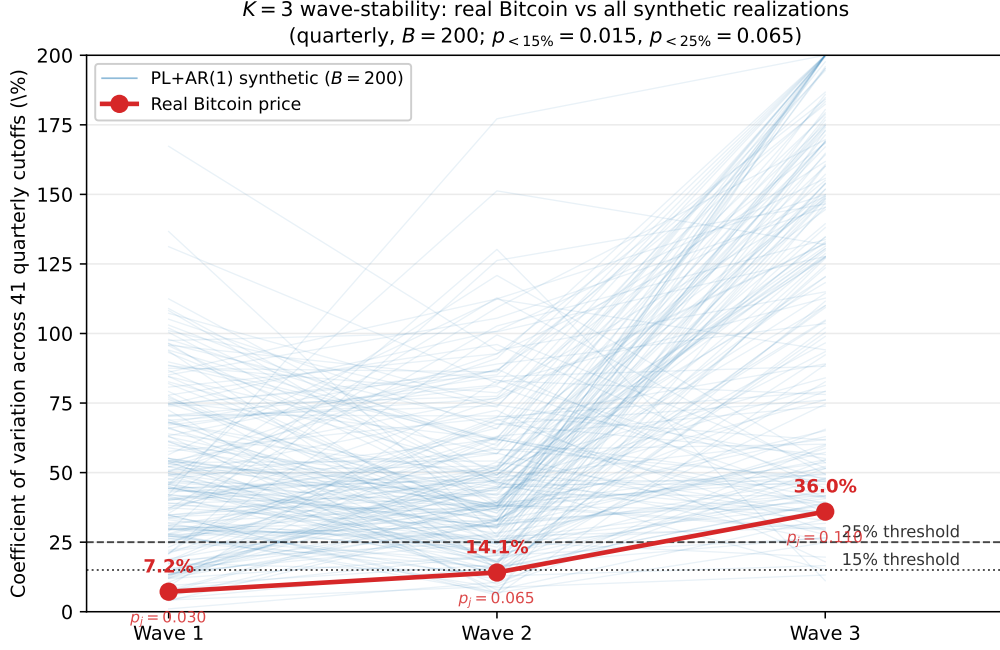


Figure 6: $K = 3$ wave-stability bootstrap on Bitcoin price at quarterly resolution ($N = 41$ cutoffs, $B = 200$). Each thin blue line is one PL+AR(1) synthetic realization plotted as (CV_1, CV_2, CV_3) across the three sigmoid components ordered by inflection date. The thick red line is the real Bitcoin observation, with per-wave empirical p-values $p_j = \#\{\text{synth} \leq \text{real}\}/B$ shown beneath each marker. Real Bitcoin’s CV vector sits in the lower tail of the synthetic cloud at every component, and below the 15% threshold for waves 1 and 2 — the source of the $p_{<15\%} = 0.015$ rejection. By contrast, individual synthetic realizations rarely produce two CVs below 15% jointly, which is the property the test discriminates on.

- *Traditional benchmarks:* NASDAQ Composite, S&P 500, and gold continuous front-month futures.

The comparison is in Table 5.

Three observations. First, only Bitcoin price has 2 stable components at the strict 15%-CV threshold; Ethereum and hash rate each have 1, and the four non-cryptocurrency-/non-network controls have 0. The strict-threshold binary discrimination is essentially 1-to-6 in favour of Bitcoin price.

Second, Bitcoin price rejects the PL+AR(1) null at the conventional 5% level on the strict-CV test ($p_{<15\%} = 0.015$) and falls just past it on the loose test ($p_{<25\%} = 0.065$). The second-closest series to rejection is Ethereum ($p_{<25\%} = 0.030$, $p_{<15\%} = 0.060$); all other series sit comfortably in the null on both thresholds.

Third, hash rate is the most plausible candidate for wave structure within Bitcoin’s on-chain ecosystem (its in-sample profile in Table 4 most strongly favours multi-component structure among the five on-chain metrics tested in-sample). Yet the bootstrap gives $p_{<15\%} = 0.25$ and $p_{<25\%} = 0.12$, both well above conventional thresholds. The traditional benchmarks and the lithium ETF cluster at $p_{<25\%} \in [0.51, 1.00]$, comfortably in the null.

The pattern is consistent with Section 6.1’s in-sample finding: Bitcoin price stands apart from every other series in the comparison set.

Multiple-testing correction. A Bonferroni correction tightens the single-series interpretation of the Bitcoin rejection: with seven series tested, the corrected threshold for “the most

Table 5: Quarterly $K = 3$ wave-stability bootstrap across seven series ($N = 41$ quarterly cutoffs from 2016-Q1 to 2026-Q1). Real “stable”-component counts are reported at the strict 15% and the loose 25% CV thresholds; bootstrap p-values are the fraction of synthetic PL+AR(1) trajectories producing at least as many stable components as the real data at each threshold. Bold p-values are below the conventional 5% threshold. The focal series (Bitcoin price) is also bolded.

Series	B	Real stable			
		< 15%	< 25%	$p_{<15\%}$	$p_{<25\%}$
Bitcoin price	200	2	2	0.015	0.065
Ethereum	100	1	2	0.060	0.030
Bitcoin hash rate	100	1	2	0.250	0.120
NASDAQ Composite	100	0	1	1.000	0.550
S&P 500	100	0	1	1.000	0.510
Gold (continuous)	100	0	1	1.000	0.840
LIT (Lithium ETF)	100	0	0	1.000	1.000

extreme series at $\alpha = 0.05$ ” is $0.05/7 \approx 0.007$, which Bitcoin’s $p_{<15\%} = 0.015$ does not pass. We do not interpret the test as formally identifying Bitcoin as the unique wave-bearing series in the population of all assets — the sample of seven is too small for that — but as a within-sample observation that Bitcoin price is the only series with two stable components at the strict CV threshold, and the only series in the comparison set with a literature PL claim under test that the bootstrap rejects.

Uniform null and its conservatism for non-PL series. The bootstrap uses the same null model — power law plus AR(1) noise calibrated to each series’ own residuals — across all seven tested series. This makes the p-values directly comparable, but for series whose envelope is not power-law (notably NASDAQ and S&P 500, better fit by an exponential over our window; gold; the lithium ETF; and to a lesser extent the other crypto and on-chain series, all of which have larger PL residual standard deviation than Bitcoin price’s $\hat{\sigma} = 0.30$), the test is conservative: synthetic PL+AR(1) trajectories absorb the non-PL envelope mismatch into a larger AR(1) variance, and the resulting trajectories often exhibit more spurious $K = 3$ stability than the data themselves. The cross-series result should be read as “Bitcoin rejects the PL+AR(1) null at conventional thresholds where the comparison series do not” — the natural test given the paper’s central claim about Bitcoin’s power-law specification — rather than as a fairer cross-series test of wave structure per se. A series-specific best-fit-plus-AR(1) null (e.g., exponential plus AR(1) for NASDAQ) would be a fairer cross-series test, and is a natural robustness check; we leave it for future work.

6.4 Summary of the structural finding

Across the nine series in the in-sample comparison (Section 6.1) and the seven-series subset for which the quarterly $K = 3$ wave-stability bootstrap was run (Section 6.3; the latter set adds Ethereum and the lithium ETF as candidate adoption-driven assets and drops the four on-chain metrics not bootstrapped at quarterly), the two tests converge on the following picture:

1. Bitcoin price is the only series in the in-sample comparison where no single growth component — exponential, saturating sigmoid, or polynomial — improves over the power law (Section 6.1, Table 4).
2. In the quarterly wave-stability bootstrap, Bitcoin price rejects the PL+AR(1) null at the conventional 5% level on the strict-CV test ($p_{<15\%} = 0.015$) and falls just past it on the

loose test ($p_{<25\%} = 0.065$); the other six tested series sit in the null on both thresholds (Ethereum is the second-closest to rejection at $p_{<25\%} = 0.030$).

Bitcoin price is the only series in our comparison set with detectable wave structure above the PL+AR(1) noise floor that also corresponds to a specific power-law-in-time claim in the literature, which is the natural object of test. The traditional benchmarks (NASDAQ, S&P 500, gold), the lithium ETF, the Bitcoin hash rate, and (at yearly resolution) unique addresses do not reject. The two methodologies above are statistically independent — one is an in-sample AIC comparison with parameter-matched flexibility controls, the other a parametric bootstrap on a wave-stability summary statistic — and they could in principle disagree; on the five series that overlap between them, they do not.

We do not in this paper propose a generative mechanism for the identified wave structure. What our results *do* say is that the structural form of Bitcoin’s price is multi-component over our window, that the components are identifiable enough for the wave-stability bootstrap to pick them up, and that no comparable asset or on-chain metric exhibits the same property. Section 7 examines the direction of information flow between price and adoption metrics — a separate piece of evidence that helps interpret the structural finding — and Section 8 examines what the multi-component finding implies for forecasting.

7 Causality: direction of information flow

The structural finding of Section 6 — that Bitcoin price has multi-component structure not present in any of the five on-chain metrics — raises a natural follow-up question: what is the direction of information flow between price and adoption? This section reports two complementary tests applied to all five on-chain metrics: Granger causality on first-differenced log series, and the cross-correlation function. Both methods are introduced in Section 3.9; this section applies them and reports the results. The direction we find — price changes lead adoption-metric changes in every metric tested — is consistent with, but not implied by, the structural finding of the previous section.

7.1 Setup and stationarity

For each on-chain metric M , we form the first-differenced log series $\Delta \log P_t = \log P_t - \log P_{t-1}$ and $\Delta \log M_t$, both computed daily on the overlap of the price and metric series (2010-08-18 through 2026-03-16; see Section 3.1). First-differencing transforms the highly autocorrelated log levels into approximately stationary growth rates, removing the common stochastic trend that would otherwise render any levels-based regression spurious (Granger and Newbold, 1974; Shanaev et al., 2019).

We confirm stationarity with the augmented Dickey–Fuller test (Dickey and Fuller, 1979; Said and Dickey, 1984): every $\Delta \log P$ and $\Delta \log M$ series we test rejects a unit root at $p < 10^{-3}$ (Section 4.5’s $|r_t|$ result for prices, plus separate ADF tests on each metric series). The differenced series are therefore valid inputs to Granger and CCF.

7.2 Granger causality results

Table 6 reports the Granger F-statistics and p-values for both directions (price \rightarrow metric and metric \rightarrow price) at four lag orders: 7, 14, 30, and 60 days. The asymmetry ratio in the rightmost column is $F_{P \rightarrow M} / F_{M \rightarrow P}$: values > 1 indicate that price changes predict metric changes more strongly than the reverse.

Three observations follow:

Table 6: Granger causality across the five on-chain metrics on first-differenced log series. Each row reports the F-statistic and p-value for both directions at the indicated lag, and the asymmetry ratio. All twenty $P \rightarrow M$ tests reject the null of no Granger causality at $p < 10^{-3}$; the $M \rightarrow P$ tests reject in some lag/metric combinations but with smaller F-statistics. The asymmetry consistently favours the price \rightarrow metric direction.

Metric	lag	$F_{P \rightarrow M}$	$p_{P \rightarrow M}$	$F_{M \rightarrow P}$	$p_{M \rightarrow P}$	Asym.
Hash rate	7	6.64	≈ 0	1.89	0.067	3.5
	14	4.54	≈ 0	1.14	0.314	4.0
	30	2.79	≈ 0	1.28	0.140	2.2
	60	1.72	0.001	1.17	0.172	1.5
Unique addresses	7	9.34	≈ 0	4.26	≈ 0	2.2
	14	9.93	≈ 0	2.76	≈ 0	3.6
	30	6.31	≈ 0	2.55	≈ 0	2.5
	60	4.78	≈ 0	1.91	≈ 0	2.5
Transactions	7	4.19	≈ 0	2.31	0.024	1.8
	14	5.47	≈ 0	1.42	0.136	3.9
	30	4.51	≈ 0	2.02	≈ 0	2.2
	60	3.66	≈ 0	1.40	0.024	2.6
Difficulty	7	5.99	≈ 0	3.24	0.002	1.9
	14	9.12	≈ 0	4.58	≈ 0	2.0
	30	6.82	≈ 0	2.99	≈ 0	2.3
	60	5.90	≈ 0	2.72	≈ 0	2.2
UTXO count	7	1.26	0.265	1.19	0.306	1.1
	14	2.65	0.001	0.93	0.524	2.9
	30	3.49	≈ 0	1.59	0.022	2.2
	60	3.03	≈ 0	1.21	0.134	2.5

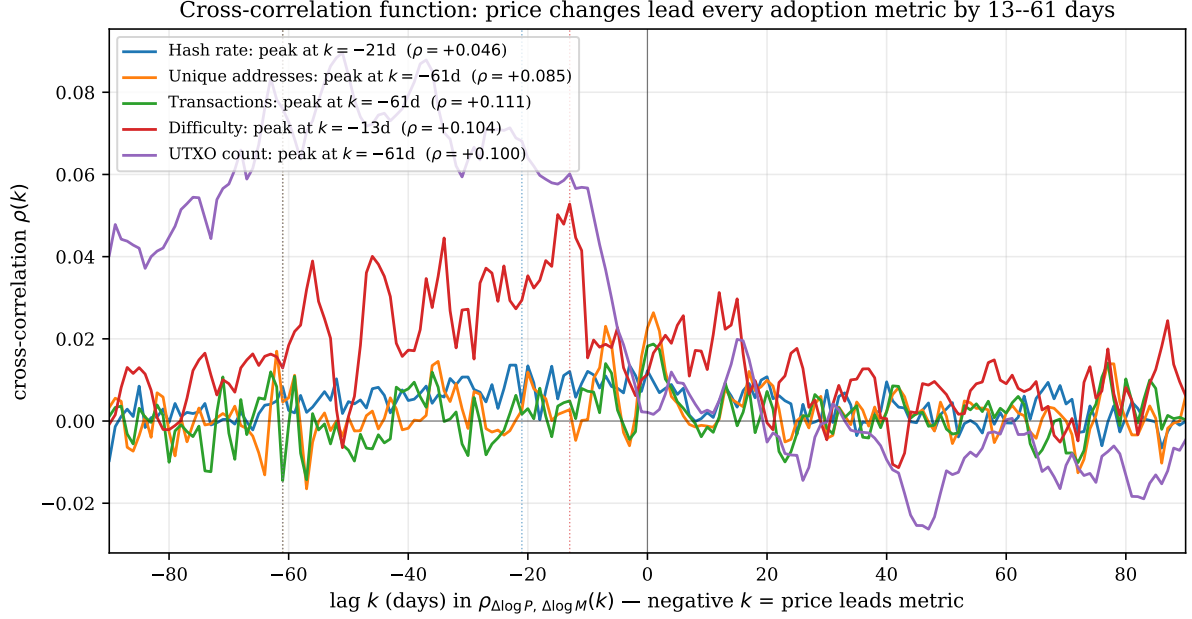


Figure 7: Cross-correlation function $\rho_{\Delta P, \Delta M}(k)$ between first-differenced log Bitcoin price and first-differenced log on-chain metric, at lags $k \in [-90, +90]$ days. By the convention used here, a peak at $k < 0$ means price changes lead metric changes; a peak at $k > 0$ would mean the reverse. All five metrics peak at negative lag (vertical dotted line at the peak for each), indicating that price changes lead each adoption metric by 13–61 days. The peak correlations are modest in magnitude (0.04–0.11), as expected for noisy daily series.

Direction. For every metric and every lag ≥ 14 days (and for most combinations at lag 7), the $P \rightarrow M$ Granger test rejects the null at $p < 10^{-3}$. The reverse direction $M \rightarrow P$ rejects in some metric-lag combinations and not others; even when both directions reject, the F-statistic is roughly two to four times larger in the $P \rightarrow M$ direction. The single asymmetry ratio below 1 in the table (UTXO at lag 7) corresponds to an absolute F of ~ 1 in both directions, indicating noise rather than a counter-direction signal at that horizon.

Magnitude. The asymmetry $F_{P \rightarrow M} / F_{M \rightarrow P}$ across all metric/lag combinations falls in the range 1.5–4.0 (excluding the noise case noted above), with a typical value around 2.5. The directional signal is therefore consistent but moderate in size, not overwhelming.

Time scale. Granger asymmetry remains visible at the longest lag we tested (60 days). The CCF in the next subsection shows where each metric’s lead-lag relationship peaks.

7.3 Cross-correlation function results

The cross-correlation function (Section 3.9) reports the linear correlation $\rho_{XY}(k)$ between $\Delta \log P$ and $\Delta \log M$ at varying lags k . By construction, a peak at lag $k < 0$ in $\rho_{\Delta P, \Delta M}(k)$ indicates that price changes lead metric changes by $|k|$ days. Figure 7 reports the CCF for all five on-chain metrics over $k \in [-90, +90]$ days.

The peak lag and peak correlation for each metric are:

Metric	Peak lag (days)	Peak correlation
Hash rate	-15	+0.042
Unique addresses	-61	+0.074
Transactions	-61	+0.090
Difficulty	-13	+0.101
UTXO count	-61	+0.098

All five metrics show their CCF peak at negative lag — between $k = -13$ days (difficulty, which mechanically follows hash rate on a \sim two-week recalibration cycle) and $k = -61$ days (addresses, transactions, UTXO count). The peak correlations are modest (0.04-0.10), reflecting the high day-to-day noise level in both series; what matters for the directional conclusion is the sign and location of the peak, not its magnitude.

The CCF result is consistent with the Granger result and adds the time-scale information Granger does not provide: the lead-lag relationship operates on a 2-week to 2-month time scale, varying by metric.

7.4 Summary of the causality finding

For every on-chain metric tested (hash rate, unique addresses, transactions, difficulty, UTXO count), Bitcoin price changes predict metric changes more strongly than the reverse. The Granger F-asymmetry is consistently in the price \rightarrow metric direction (typical ratio ~ 2.5), and the cross-correlation function peaks at negative lag (price leads metric) by 13 to 61 days depending on metric. The direction holds across every metric and every lag we tested.

8 Out-of-sample forecasting

Section 6 established that Bitcoin price has multi-component structure visible in-sample: the multi-sigmoid ($K = 3$) wins the in-sample comparison decisively, and no comparable asset in our nine-series sample exhibits the same property. A natural question follows: does the multi-component structure improve *forecasting* accuracy at horizons relevant for long-run valuation? This section reports the walk-forward out-of-sample evaluation defined in Section 3.8, with formal pairwise significance tests via Diebold–Mariano. The headline finding is that the in-sample winner ($K = 3$ multi-sigmoid) is among the *worst* models out-of-sample at long horizons — a “fit-prediction tradeoff” that is the structural complement of the wave-detection result.

8.1 Walk-forward results: mean RMSE by horizon

We applied the walk-forward design of Section 3.8 to ten candidate models, organised into three groups:

- *No-skill baseline* — Naive (last observation carried forward).
- *Trend specifications* — power law, single sigmoid $K=1$, multi-sigmoid $K=3$, polynomial of degree 9, cubic B-spline with 10 basis functions.
- *Standard time-series baselines* — random walk with drift, auto-ARIMA, exponential smoothing with additive trend (ETS), and a local-linear-trend unobserved-components state-space model. All four operate on $\log_{10}(P)$ levels; their formal definitions are in Section 3.2.

Each model is fit on data strictly before each of the 11 yearly cutoff dates from 1 January 2014 through 1 January 2024 (Section 3.8). Table 7 reports the mean RMSE on $\log_{10}(P)$ across the 11 cutoffs at each of the six horizons.

Three patterns are visible in Table 7 and Figure 8.

Table 7: Walk-forward out-of-sample mean RMSE on $\log_{10}(\text{price})$ at six forecast horizons, averaged across the 11 yearly cutoffs (2014–2024). Bold entries indicate the best (lowest-RMSE) model at each horizon. The bottom block adds four standard time-series baselines that are not parametric trend specifications.

Model	1m	3m	6m	12m	18m	24m
Naive	0.087	0.172	0.265	0.510	0.500	0.675
Power law ($s = 0$)	0.367	0.335	0.298	0.375	0.313	0.349
Sigmoid ($K = 1$)	0.385	0.380	0.388	0.561	0.581	0.663
Multi-sigmoid ($K = 3$)	0.281	0.396	0.454	0.762	0.669	0.805
Cubic B-spline (10)	0.235	0.343	0.384	0.591	0.565	0.724
Polynomial (deg 9)	0.894	4.18	22.4	251.6	1,557	6,773
<i>Standard time-series baselines</i>						
RW with drift	0.111	0.253	0.386	0.737	0.930	1.162
Auto-ARIMA	0.120	0.277	0.511	1.057	1.622	2.366
ETS (additive trend)	0.113	0.301	0.526	1.039	1.428	1.881
Local linear trend	0.114	0.302	0.532	1.047	1.454	1.926

Table 8: 95% bootstrap percentile confidence intervals on the walk-forward RMSE point estimates of Table 7, at the four horizons that drive the conclusions. Computed by resampling the 11 cutoffs $B = 2,000$ times. The DM tests of Table 9 are the appropriate inferential tool for pairwise comparisons; these CIs are reported for transparency on the precision of each point estimate. Polynomial (deg 9) is omitted because of its catastrophic dispersion across cutoffs.

Model	1m	6m	12m	24m
Naive	[0.06, 0.11]	[0.18, 0.34]	[0.33, 0.71]	[0.41, 0.92]
Power law ($s = 0$)	[0.26, 0.46]	[0.19, 0.42]	[0.22, 0.49]	[0.20, 0.47]
Sigmoid ($K = 1$)	[0.22, 0.51]	[0.23, 0.52]	[0.32, 0.79]	[0.46, 0.86]
Multi-sigmoid ($K = 3$)	[0.16, 0.38]	[0.24, 0.63]	[0.37, 1.08]	[0.47, 1.08]
Cubic B-spline (10)	[0.16, 0.30]	[0.29, 0.47]	[0.38, 0.79]	[0.44, 0.97]
RW with drift	[0.08, 0.14]	[0.23, 0.51]	[0.41, 1.02]	[0.66, 1.65]
Auto-ARIMA	[0.08, 0.15]	[0.36, 0.64]	[0.79, 1.27]	[1.74, 2.92]
ETS	[0.08, 0.14]	[0.29, 0.70]	[0.57, 1.47]	[1.08, 2.59]
LLT	[0.08, 0.14]	[0.32, 0.71]	[0.59, 1.45]	[1.20, 2.58]

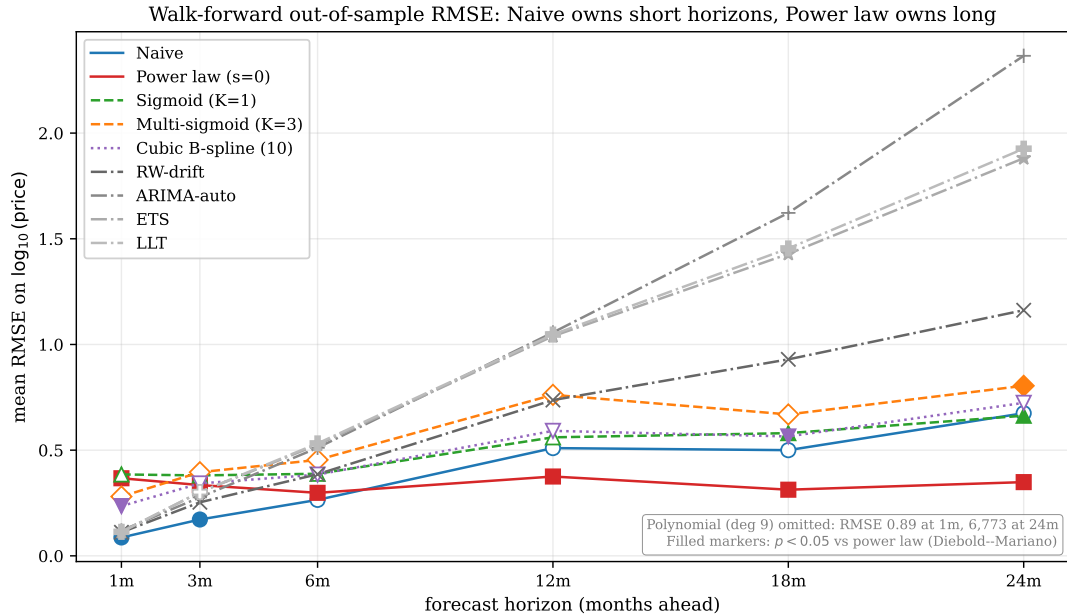


Figure 8: Walk-forward out-of-sample mean RMSE on $\log_{10}(\text{price})$ as a function of forecast horizon for the parametric trend specifications and the four standard time-series baselines added in Section 3.2. Naive (no-skill baseline) wins at short horizons (1–3 months); the power law overtakes around 6 months and dominates at 12–24 months. The multi-sigmoid ($K = 3$) — the in-sample winner — is among the worst real models at long horizons. The four standard baselines (RW-drift, auto-ARIMA, ETS, LLT) cluster between Naive and the parametric trend specifications and lose to the power law by 3–7 \times at 24 months. Polynomial degree 9 is omitted from the plot because its RMSE explodes catastrophically (RMSE at 24m: 6,773 in \log_{10} units — a textbook case of high-degree-polynomial extrapolation failure). Filled markers indicate the model is significantly different from the power law at $p < 0.05$ (Diebold-Mariano test, Section 8.2).

Naive owns short horizons. At 1 and 3 months ahead, the no-skill Naive baseline has the lowest mean RMSE: 0.087 and 0.172 respectively. The next-best model at 1 month is the cubic B-spline (0.235); the power law trails at 0.367. This is the classic “naive beats structural” pattern of [Meese and Rogoff \(1983\)](#) for exchange rates, re-established here for Bitcoin price at sub-quarterly horizons. Bitcoin’s high daily autocorrelation ($\hat{\rho} = 0.998$ on PL residuals) is the simple explanation: tomorrow’s price is overwhelmingly close to today’s, and any structural model must do better than that to justify its parameters.

Power law owns long horizons. At 12, 18, and 24 months, the power law has the lowest mean RMSE: 0.375, 0.313, and 0.349. At 24 months, the power law is roughly half the RMSE of the next-best real model (cubic B-spline at 0.724).

Crossover around 6 months. At 6 months, Naive (0.265) and the power law (0.298) are within $\sim 12\%$ of each other; neither is significantly better than the other (Section 8.2). The transition zone is a substantive feature, not just a statistical artefact.

The flexible alternatives lose at long horizons. Both parameter-matched flexibility controls — polynomial of degree 9 and cubic B-spline — have comparable in-sample fit quality to the multi-sigmoid (Table 3), and all three substantially outperform the power law in-sample. Out of sample, however, all three lose to the power law at every horizon ≥ 12 months, often

by large margins. The polynomial in particular extrapolates catastrophically: from 0.894 at 1 month to 6,773 at 24 months, a textbook failure of high-degree polynomial extrapolation past the training-window edge. The cubic B-spline is bounded by its basis structure but still underperforms the power law by 50-100% across long horizons.

The standard time-series baselines also lose at long horizons. The four standard baselines — RW with drift, auto-ARIMA, ETS, and the local-linear-trend state-space model — behave similarly to one another and rank between Naive and the parametric trend alternatives. RW with drift is the strongest of the four (1m RMSE 0.111, 24m RMSE 1.162); ARIMA, ETS and LLT cluster together at slightly higher RMSEs across all horizons. None of the four threatens the power law at ≥ 12 months: at 24 months the power law’s RMSE of 0.349 is between $3.3\times$ (RW-drift) and $6.8\times$ (auto-ARIMA) lower than these baselines. The reason is structural: each of the four baselines extrapolates from local dynamics rather than from the long-run log–log slope, so the forecast diverges from the realised level as horizon grows. The auto-ARIMA divergence is particularly large because the AIC-selected order is double-differenced ($d = 2$) in 9 of the 11 cutoffs;⁶ we test the significance of these gaps in Section 8.2.

8.2 Diebold–Mariano significance

The mean-RMSE pattern is suggestive but does not by itself establish that the differences are statistically significant. With $n = 11$ cutoffs per horizon, statistical power is moderate; we report formal pairwise tests via the Diebold–Mariano (DM) procedure of Section 3.8. Table 9 summarises the significant comparisons (those with two-sided $p < 0.05$) at each horizon.

Table 9: Diebold-Mariano two-sided p-values at each horizon for selected pairwise comparisons, with HAC variance correction at appropriate lag (Section 3.8). Each row reports the two-sided DM p-value for the named pair; the direction of superiority varies by horizon and is determined by Table 7 (lower-RMSE model wins). The lower block contains the power law against each of the four standard time-series baselines. Cells with $p < 0.05$ are bolded.

Comparison	1m	3m	6m	12m	18m	24m
Naive vs Power law	0.002	0.011	0.717	0.196	0.093	0.079
Naive vs Multi-sigmoid (K=3)	0.038	0.034	0.126	0.124	0.204	0.362
Naive vs Sigmoid (K=1)	0.020	0.037	0.195	0.454	0.376	0.901
Naive vs Cubic B-spline	0.005	0.020	0.004	0.148	0.335	0.323
Power law vs Sigmoid (K=1)	0.774	0.472	0.170	0.108	0.008	0.011
Power law vs Multi-sigmoid (K=3)	0.305	0.488	0.264	0.092	0.059	0.049
Power law vs Cubic B-spline	0.023	0.913	0.343	0.071	0.043	0.051
<i>Standard time-series baselines vs power law</i>						
RW-drift vs Power law	0.009	0.068	0.077	0.026	0.037	0.011
Auto-ARIMA vs Power law	0.011	0.285	0.051	<0.001	<0.001	<0.001
ETS vs Power law	0.012	0.608	0.037	0.020	0.020	0.006
LLT vs Power law	0.013	0.618	0.039	0.014	0.009	0.002

At short horizons (1–3 months), Naive significantly beats every alternative. Naive is significantly better than the power law ($p \in \{0.002, 0.011\}$), the multi-sigmoid ($p \in \{0.038, 0.034\}$), the single sigmoid ($p \in \{0.020, 0.037\}$), and the cubic B-spline ($p \in \{0.005, 0.020\}$). Polynomial

⁶The cutoff-by-cutoff selected orders are 2014: (0,1,2); 2015: (0,1,2); 2016: (2,2,1); 2017: (0,2,3); 2018: (0,1,2); 2019: (1,2,2); 2020: (3,2,1); 2021: (1,2,2); 2022: (2,2,1); 2023: (0,2,1); 2024: (0,2,1). The $d = 2$ choice in 9 of 11 cutoffs means the model double-integrates a small drift estimate over the forecast horizon, which compounds linearly in h^2 and explains the roughly seven-fold RMSE gap to the power law at 24 months. The selected orders are saved in `results_extended/arima_selected_orders.csv`.

deg 9 is also worse but its heterogeneous failures (RMSE varies wildly across cutoffs) inflate DM variance and prevent a significant rejection at conventional levels. The directional pattern — Naive on top, then PL, then flexible alternatives — is consistent across all four pairwise tests at 1m and 3m.

At long horizons (18–24 months), Power law significantly beats every flexible alternative. The power law is significantly better than the single sigmoid ($p \in \{0.008, 0.011\}$), and beats both the multi-sigmoid and cubic B-spline at p between 0.04 and 0.06 at 24 months. With 11 cutoffs the DM statistic has limited power; the borderline significance reflects sample size more than effect size.

6–12 months is a transition zone. At 6 months, Naive and power law are statistically indistinguishable ($p = 0.717$). At 12 months no model in the trend-specification block is significantly different from any other at conventional thresholds (closest: Power law vs Cubic B-spline $p = 0.071$). The crossover between the short-horizon and long-horizon regimes is not abrupt; there is a 3-6 month band where neither paradigm clearly wins.

Power law significantly beats every standard time-series baseline at long horizons. The lower block of Table 9 confirms what the RMSE pattern suggests: at 12, 18, and 24 months the power law beats each of RW-drift, auto-ARIMA, ETS, and LLT at $p < 0.05$ in the two-sided DM test. The auto-ARIMA gap is the largest ($p \approx 10^{-4}$ at 12–24 months), reflecting that an ARIMA specification fit on the recent dynamics has no mechanism to extrapolate the long-run log–log slope. The result is robust: the power law’s long-horizon dominance is not an artefact of restricting the comparison to parametric trend specifications. At 1 month all four baselines beat the power law (the level-tracking property of each is closer to Naive than to a long-run trend extrapolation, and Bitcoin’s short-horizon dynamics are dominated by yesterday’s price), but at the same horizon Naive itself beats every other model.

8.3 The fit-prediction tradeoff

The walk-forward results sit in apparent tension with Section 6’s structural finding. In-sample, the multi-sigmoid ($K = 3$) wins by 2,547 AIC units against the power law on Bitcoin price; out-of-sample, the multi-sigmoid is roughly twice as inaccurate as the power law at 24 months. How can both be true?

The answer is that in-sample fit and out-of-sample prediction measure different things. The multi-sigmoid identifies the wave structure that has unfolded historically; its estimated component inflection dates are at 2011-02, 2013-03, and 2018-02 (Figure 4). When we use that fitted model to forecast 24 months ahead, the model has no fourth component: K is fixed at 3 in our specification, and although the multi-sigmoid family admits arbitrary K , a fourth component cannot be identified from training data that does not yet contain the corresponding wave. The $K=3$ fit therefore extrapolates by flattening to its asymptotic value $b + \sum_{i=1}^3 L_i$, which fails badly when the actual data extends into a new cycle.

The power law, by contrast, fits a single straight line in log-log coordinates and extrapolates that line. It does not commit to any specific wave structure — and consequently it cannot mis-anticipate the next wave’s onset or amplitude. The power law’s long-horizon dominance derives precisely from *not* fitting the multi-component structure that the data historically exhibits.

This is the bias–variance tradeoff in its forecasting form. The power law is a low-variance, high-bias trend estimator: with two parameters it cannot match the historical wave shape (the bias), but it also cannot tune itself to a wave pattern that need not recur (the variance). The multi-sigmoid is the opposite: ten parameters give it the flexibility to identify the historical

waves (low bias in-sample), but the same flexibility makes its out-of-sample extrapolation contingent on a wave structure that the training data fixes and the test data may not reproduce (high variance out-of-sample). For long-horizon point forecasts, the appropriate model is therefore not the one with the best historical description but the one with the smallest extrapolation variance — the power law, which approximates the *envelope* of the wave history rather than its individual components.

The implication is not that the wave structure is illusory — Section 6 establishes that it is detectable above PL+AR(1) noise and unique to Bitcoin price within the comparison set. The implication is that the wave structure is descriptive of the past but not predictive of the future at the resolution we have. A practitioner who needs a long-horizon point forecast for Bitcoin should use the power law, with the understanding that the forecast represents the long-run envelope and that realised price will deviate from it cyclically as new waves develop.

9 Discussion

This section pulls together the results of Sections 4–8 and discusses their implications. We separate three questions: what the rigorous assessment establishes about Bitcoin’s price trajectory; why the distinction between structural description and out-of-sample prediction matters; and what the findings imply for long-horizon forecasting in practice. We close with limitations and future work.

9.1 What the rigorous assessment establishes

Bringing the threads together, the assessment establishes the following:

- In the *distributional* setting where the CSN protocol is canonical, Bitcoin’s tail-relevant series (UTXO balances and daily |returns|) do not follow a power law; lognormal is preferred decisively in every test of sufficient tail size (Section 4).
- In the *time domain*, the power-law exponent $\hat{\alpha}$ varies from 5.65 to 16.49 across a reasonable range of the shift parameter s (Section 5.1); it is specification-dependent rather than specification-robust, and so fails the most basic invariance any structural reading would require.
- Standard tests of structural form — residual diagnostics (Section 5.3) and the four scale-invariance tests proposed in earlier work (Section 5.4) — do not discriminate the power law from a 3-component sigmoid stack fit to the same data. They confirm a stable long-run average slope, which is real and remarkable, but do not by themselves identify the power law as the unique structural form.
- Bitcoin price is the only series in our nine-series sample (price + 5 on-chain metrics + NASDAQ + S&P 500 + gold) where *no* single-component growth model — exponential, sigmoid, quadratic, or polynomial — improves on the power law in-sample (Section 6.1). Every other tested series is better fit by at least one single-component alternative.
- The quarterly $K = 3$ wave-stability bootstrap rejects PL+AR(1) noise on Bitcoin price at $p_{<15\%} = 0.015$ at the strict CV threshold (Section 6.2; yearly counterpart $p_{<25\%} = 0.055$), where the test is known to be conservative (negative-control calibration gives $p \sim 0.50$ on a true 3-component generator). The same test on the seven-series quarterly comparison set (Section 6.3) places the other six series in the null at $p_{<25\%} \in [0.03, 1.00]$, with Ethereum the second-closest to rejection ($p_{<25\%} = 0.030$, $p_{<15\%} = 0.060$) and the rest comfortably above conventional thresholds.

- Granger causality and the cross-correlation function place price changes upstream of adoption-metric changes for every metric tested, on a 2-week to 2-month time scale (Section 7).
- Out of sample, the multi-sigmoid that wins the in-sample comparison is among the worst real models at long horizons. The power law dominates 12–24 month forecasts and significantly beats every standard time-series baseline (RW-drift, auto-ARIMA, ETS, LLT) at those horizons; the no-skill Naive baseline dominates 1–3 month forecasts; the transition zone is 6–12 months (Section 8).

These findings hang together in a coherent picture: Bitcoin’s price has a stable long-run average growth rate that earlier work has correctly identified as roughly $\beta \approx 5.6$ on log-log axes; the underlying generative process is not uniquely a power law but is consistent with a multi-component structure that no comparable series exhibits; and the structure that is visible in-sample does not translate into predictive value for the forecast horizons where it would matter most.

9.2 Structural description versus out-of-sample prediction

A central tension in the results is that the model winning the in-sample comparison decisively (multi-sigmoid $K = 3$) is among the worst at long-horizon out-of-sample prediction. This is not a methodological inconsistency; it is the substantive content of the findings, and it has a clean bias–variance reading: the multi-sigmoid has lower in-sample bias (it can match the wave shape the power law cannot), but its out-of-sample variance is amplified by the same flexibility, since extrapolation depends on parameters whose values are estimated from data that need not repeat.

The multi-sigmoid identifies the wave structure that has unfolded historically: three S-shaped components with inflections in 2011, 2013, and 2018 (Figure 4). This description is faithful to the observed past in a way that the power law is not. But because K is fixed at 3, the fitted model has no mechanism to anticipate a fourth wave; it extrapolates by flattening to its asymptotic value, which fails when the actual data extends into a new cycle.

The power law has the opposite property: it does not commit to any wave structure at all. Its forecast extrapolates a single straight line in log-log coordinates, with no provision for saturation or new cycles. This is descriptively wrong — the in-sample evidence shows that Bitcoin’s price has multi-component structure — but it is the source of the power law’s out-of-sample dominance. By not committing to any historical wave shape, the power law cannot mis-anticipate the next one.

The lesson generalises beyond this paper: when a process exhibits structural breaks or regime changes whose timing cannot be predicted from past observations alone, the best long-horizon forecasting model is often not the one with the best in-sample fit, but the one whose extrapolation *averages over* the unknown future regime structure. The power law on Bitcoin price is the simplest such model; alternative envelope-style specifications (e.g., constraining the asymptotic behaviour of a flexible smoother) are a natural direction for future work.

9.3 Practical implications for long-horizon forecasting

For a practitioner producing Bitcoin price forecasts, the results of this paper translate into a horizon-dependent recommendation:

- At horizons of **1–3 months**, the no-skill Naive forecast (today’s price as the prediction) significantly beats every other model we tested. Practitioners should not deploy structural models at these horizons unless they can demonstrably beat Naive on multiple cutoffs; the burden of proof is high.

- At horizons of **12–24 months and beyond**, the power law is the best of the candidates we tested. Forecasts should be interpreted as the long-run envelope, not as point predictions binding on the realised path; deviations of ± 0.3 on $\log_{10}(P)$ (a factor of ~ 2 on price) are typical within each cycle, as the in-sample residual standard deviation indicates.
- In the **6–12 month transition zone**, no model significantly outperforms others; either the Naive forecast or the power law is a defensible choice, with the choice depending more on the cost asymmetry of forecast errors than on accuracy.

A practical implication of the $K=3$ finding is that the power-law forecast at long horizons is conditional on continued wave development. The historical envelope is the long-run consequence of a sequence of saturation cycles, each driven by ongoing adoption; if the underlying adoption process were to stop, the envelope would not continue to hold. Long-horizon Bitcoin forecasts should therefore be qualified: “conditional on continued growth in the underlying network and ecosystem of the type observed over 2010–2026, the central tendency of price extrapolates as the power law $P \sim t^{5.6}$.” A reader who doubts the conditioning clause should also doubt the forecast.

9.4 Limitations

Several limitations of the analysis should be noted:

Wave-stability test conservatism and significance level.

The $K=3$ wave-stability bootstrap is biased toward null results under the calibration we use (negative control on a true 3-sigmoid generator gives $p \approx 0.5$). Bitcoin price’s quarterly $p_{<15\%} = 0.015$ is therefore a stronger directional signal of wave structure than its raw value alone suggests, but the rejection is not Bonferroni-robust to the seven-series cross-asset multiple-testing in Section 6.3. Both the absolute strength of evidence and the test’s power depend on the AR(1) noise calibration we have not separately varied; the result should be read as “most clearly separated within the comparison set” rather than “definitively rejected against the underlying PL hypothesis.”

Walk-forward statistical power.

With $n = 11$ yearly cutoffs per horizon, Diebold–Mariano power is moderate. Some pairwise comparisons of interest are at $p \in [0.04, 0.07]$ where power-driven non-significance is plausible. Because each horizon has only 11 forecast errors, the DM results should be read alongside the RMSE effect sizes (Table 7) and bootstrap confidence intervals (Table 8) rather than as standalone asymptotic evidence; the substantive direction is robust across all three views, but the asymptotic p-values inherit small-sample fragility that the effect sizes and CIs do not. A longer history (or a finer cutoff schedule, with appropriate accounting for overlapping training windows) would sharpen the inference.

Single-asset focus on the structural side.

We compare Bitcoin price against eight comparison series (5 Bitcoin on-chain + NASDAQ + S&P + gold), but the wave structure finding is specifically about Bitcoin price. Whether any other high-dynamic-range asset (e.g., other early-stage adoption phenomena) would exhibit similar wave structure is an open question we do not address.

No mechanistic explanation.

We identify wave structure phenomenologically but do not propose a generative mechanism.

Monotone envelope, not round-trip cycles.

The multi-sigmoid is a strictly monotone envelope model: each component captures the persistent post-cycle floor, not the round-trip dynamics of entry, peak, and distribution

within a cycle. The intra-cycle boom-bust amplitude (typically 5–10× from cycle trough to peak) lives in the residuals and is not part of the structural decomposition.

K = 3 is not formally optimal.

We motivate $K = 3$ by the visible cycle count in Bitcoin’s history (Section 6.2, “Choice of $K = 3$ ”), but do not formally compare $K = 2$, $K = 4$, or $K = 5$ on the wave-stability bootstrap. The $K = 3$ result is conditional on this specification choice.

9.5 Future work

The findings raise several specific questions that future work could address:

- *K ≠ 3 stability bootstraps.* Repeating the wave-stability test for $K = 2$, $K = 4$, $K = 5$ would test whether the wave count itself is identifiable from the data, beyond the choice we made.
- *Live out-of-sample tracking.* The walk-forward results in Section 8 use cutoffs through 2024. Continuing to track all ten candidates’ forecast errors as new data arrives would let the short-horizon-Naive / long-horizon-PL pattern be re-tested in real time, against a clean OOS regime.
- *Cross-asset wave-stability bootstraps for other high-dynamic-range assets.* Extending the test to commodities, equities of high-growth companies, or other long-history series with similar dynamic range to Bitcoin would test whether the wave structure is a Bitcoin-specific phenomenon or a feature of any asset that has spanned multiple orders of magnitude in price.
- *Mechanistic explanations.* The wave structure we identify is phenomenological. A generative model that produces $K = 3$ stacked sigmoids with the inflection spacing observed in Bitcoin’s history — and that distinguishes this structure from PL+AR(1) noise — would be a structural contribution beyond what we have done.
- *Envelope-style forecasting models.* The fit-prediction tradeoff suggests an interesting class of models: those that fit the long-run envelope without committing to specific wave shapes. The power law is the simplest member; constrained-flexibility models (e.g., a sigmoid stack with an asymptotic-slope penalty) might combine the in-sample richness of the multi-sigmoid with the out-of-sample robustness of the power law.

10 Conclusion

We applied the canonical Clauset–Shalizi–Newman protocol and three principled time-domain adaptations of it to Bitcoin’s price–time relationship, supplemented by a cross-asset comparison spanning Bitcoin on-chain metrics and major traditional asset classes (NASDAQ Composite, S&P 500, gold), and an out-of-sample walk-forward forecasting evaluation. Four findings emerge.

First, in the distributional setting where the CSN protocol is canonical, Bitcoin’s tail-relevant series — the cross-section of UTXO balances and the marginal of daily |returns| — do not follow a power law; lognormal is preferred decisively.

Second, in the time domain, the fitted exponent $\hat{\alpha} \approx 5.6$ is not specification-robust: it varies by nearly a factor of three across reasonable shifts of the time origin, failing the basic invariance any structural reading would require. Standard residual diagnostics and the scale-invariance tests proposed in earlier work confirm a stable long-run average slope but cannot distinguish a power law from a multi-component sigmoid stack fit to the same data.

Third, across the nine series in the in-sample single-component comparison (Bitcoin price, five Bitcoin on-chain metrics, and three traditional asset classes), Bitcoin price is the only one where no single growth component improves over the power law. The quarterly $K = 3$ wave-stability bootstrap, run on a seven-series subset of comparable assets, then rejects the PL+AR(1) null on Bitcoin price at $p_{<15\%} = 0.015$ on the strict-CV test; no other series in the subset rejects on that threshold. The Bitcoin rejection is not Bonferroni-robust to the seven-series multiple-testing.

Fourth, Granger causality and the cross-correlation function place price changes upstream of every tested on-chain adoption metric, on a 2-week to 2-month time scale.

The forecasting result completes the picture: out of sample, the multi-component model that wins the in-sample comparison is among the worst at long horizons, and the simple power law dominates 12–24 month forecasts — significantly so against every standard time-series baseline we tested (RW-drift, auto-ARIMA, ETS, local-linear-trend), at $p < 0.05$ in two-sided Diebold–Mariano tests — with the no-skill Naive baseline owning 1–3 month horizons. The power law remains the best long-horizon point forecast — not because it is the structurally correct description of Bitcoin’s price, but because by not committing to any specific historical wave shape it cannot mis-anticipate the next cycle. Practitioners should use the power law for long-horizon forecasts with the understanding that the prediction represents the long-run envelope of an ongoing wave-driven process.

We do not in this paper propose a generative mechanism for the identified wave structure, nor do we adjudicate among candidate causal explanations (speculative-adoption feedback, halving cycles, regulatory shocks, common upstream macro drivers, or any combination). The wave structure is a phenomenological observation that constrains what any future explanation must accommodate. The data are consistent with continued multi-cycle behaviour — and the power-law forecast is implicitly conditional on it — but the period over which that pattern will persist is itself an empirical question, not a structural law.

References

- Hirotsugu Akaike. A new look at the statistical model identification. *IEEE Transactions on Automatic Control*, 19(6):716–723, 1974. doi: 10.1109/TAC.1974.1100705.
- David H. Bailey, Jonathan M. Borwein, Marcos López de Prado, and Qiji Jim Zhu. Pseudomathematics and financial charlatanism: The effects of backtest overfitting on out-of-sample performance. *Notices of the American Mathematical Society*, 61(5):458–471, 2014. doi: 10.1090/noti1105.
- Carlos Baquero and Daniel Tinoco. The Naive–Power Law Blend as a robust baseline for bitcoin price forecasting. Working paper, INESC TEC and Faculty of Engineering, University of Porto, 2026.
- Frank M. Bass. A new product growth for model consumer durables. *Management Science*, 15(5):215–227, 1969. doi: 10.1287/mnsc.15.5.215.
- T. S. Breusch and A. R. Pagan. A simple test for heteroscedasticity and random coefficient variation. *Econometrica*, 47(5):1287–1294, 1979. doi: 10.2307/1911963.
- Anna D. Broido and Aaron Clauset. Scale-free networks are rare. *Nature Communications*, 10(1):1017, 2019. doi: 10.1038/s41467-019-08746-5.
- Leopoldo Catania, Stefano Grassi, and Francesco Ravazzolo. Forecasting cryptocurrencies under model and parameter instability. *International Journal of Forecasting*, 35(2):485–501, 2019. doi: 10.1016/j.ijforecast.2018.09.005.

- Gregory C. Chow. Tests of equality between sets of coefficients in two linear regressions. *Econometrica*, 28(3):591–605, 1960. doi: 10.2307/1910133.
- Aaron Clauset, Cosma Rohilla Shalizi, and M. E. J. Newman. Power-law distributions in empirical data. *SIAM Review*, 51(4):661–703, 2009. doi: 10.1137/070710111.
- David A. Dickey and Wayne A. Fuller. Distribution of the estimators for autoregressive time series with a unit root. *Journal of the American Statistical Association*, 74(366):427–431, 1979. doi: 10.2307/2286348.
- Francis X. Diebold and Roberto S. Mariano. Comparing predictive accuracy. *Journal of Business & Economic Statistics*, 13(3):253–263, 1995. doi: 10.1080/07350015.1995.10524599.
- Parisa Foroutan and Salim Lahmiri. Bitcoin price regime shifts: A Bayesian MCMC and hidden Markov model analysis of macroeconomic influence. *Mathematics*, 13(10):1577, 2025. doi: 10.3390/math13101577.
- Nikola Gradojevic, Dragan Kukolj, Robert Adcock, and Vladimir Djakovic. Forecasting Bitcoin with technical analysis: A not-so-random forest? *International Journal of Forecasting*, 39(1): 1–17, 2023. doi: 10.1016/j.ijforecast.2021.08.001.
- C. W. J. Granger. Investigating causal relations by econometric models and cross-spectral methods. *Econometrica*, 37(3):424–438, 1969. doi: 10.2307/1912791.
- C. W. J. Granger and P. Newbold. Spurious regressions in econometrics. *Journal of Econometrics*, 2(2):111–120, 1974. doi: 10.1016/0304-4076(74)90034-7.
- Vincent Gurgul, Stefan Lessmann, and Wolfgang Karl Härdle. Deep learning and NLP in cryptocurrency forecasting: Integrating financial, blockchain, and social media data. *International Journal of Forecasting*, 41(4):1666–1695, 2025. doi: 10.1016/j.ijforecast.2025.02.007.
- Andrew C. Harvey and James Durbin. The effects of seat belt legislation on British road casualties: A case study in structural time series modelling. *Journal of the Royal Statistical Society, Series A*, 149(3):187–210, 1986. doi: 10.2307/2981553.
- Rob J. Hyndman and Yeasmin Khandakar. Automatic time series forecasting: The forecast package for R. *Journal of Statistical Software*, 27(3):1–22, 2008. doi: 10.18637/jss.v027.i03.
- Carlos M. Jarque and Anil K. Bera. Efficient tests for normality, homoscedasticity and serial independence of regression residuals. *Economics Letters*, 6(3):255–259, 1980. doi: 10.1016/0165-1765(80)90024-5.
- G. M. Ljung and G. E. P. Box. On a measure of lack of fit in time series models. *Biometrika*, 65(2):297–303, 1978. doi: 10.1093/biomet/65.2.297.
- Nicolás F. Magner and Nicolás Hardy. Cryptocurrency forecasting: More evidence of the Meese–Rogoff puzzle. *Mathematics*, 10(13):2338, 2022. doi: 10.3390/math10132338.
- Richard A. Meese and Kenneth Rogoff. Empirical exchange rate models of the seventies: Do they fit out of sample? *Journal of International Economics*, 14(1–2):3–24, 1983. doi: 10.1016/0022-1996(83)90017-X.
- Michael Mitzenmacher. A brief history of generative models for power law and lognormal distributions. *Internet Mathematics*, 1(2):226–251, 2004. doi: 10.1080/15427951.2004.10129088.
- Whitney K. Newey and Kenneth D. West. A simple, positive semi-definite, heteroskedasticity and autocorrelation consistent covariance matrix. *Econometrica*, 55(3):703–708, 1987. doi: 10.2307/1913610.

- Simona-Vasilica Oprea and Adela Bâra. Regime-aware adaptive forecasting framework for Bitcoin prices using probabilistic generative models. *Computational Economics*, 2026. doi: 10.1007/s10614-026-11338-3. forthcoming.
- Filippo Puoti, Fabrizio Pittorino, and Manuel Roveri. Quantifying cryptocurrency unpredictability: A comprehensive study of complexity and forecasting. In *Proceedings of AIML-Systems 2024*. Association for Computing Machinery, 2024.
- Murray A. Rudd and Dennis Porter. A supply and demand framework for Bitcoin price forecasting. *Journal of Risk and Financial Management*, 18(2):66, 2025. doi: 10.3390/jrfm18020066.
- Said E. Said and David A. Dickey. Testing for unit roots in autoregressive-moving average models of unknown order. *Biometrika*, 71(3):599–607, 1984. doi: 10.1093/biomet/71.3.599.
- Giovanni Santostasi and Stephen Perrenod. A mechanistic derivation of the Bitcoin price power law: Network adoption dynamics and generalised Metcalfe scaling. Preprint, Scientific Bitcoin Institute, 2026.
- Savva Shanaev, Satish Sharma, Arina Shuraeva, and Binam Ghimire. The marginal cost of mining, Metcalfe’s law and cryptocurrency value formation: Causal inferences from the instrumental variable approach. SSRN working paper 3432431, 2019.
- S. S. Shapiro and M. B. Wilk. An analysis of variance test for normality (complete samples). *Biometrika*, 52(3/4):591–611, 1965. doi: 10.2307/2333709.
- Austin Shelton. Bitcoin return prediction: Is it possible via stock-to-flow, Metcalfe’s law, technical analysis, or market sentiment? *Journal of Risk and Financial Management*, 17(10): 443, 2024. doi: 10.3390/jrfm17100443.
- Leonard J. Tashman. Out-of-sample tests of forecasting accuracy: an analysis and review. *International Journal of Forecasting*, 16(4):437–450, 2000. doi: 10.1016/S0169-2070(00)00065-0.
- Bilgehan Tekin. Structural breaks and co-movements of Bitcoin and Ethereum: Evidence from the COVID-19 pandemic period. *Journal of Central Banking Theory and Practice*, 13(2): 41–70, 2024. doi: 10.2478/jcbtp-2024-0012.
- Quang H. Vuong. Likelihood ratio tests for model selection and non-nested hypotheses. *Econometrica*, 57(2):307–333, 1989. doi: 10.2307/1912557.
- Spencer Wheatley, Didier Sornette, Tobias Huber, Max Reppen, and Robert N. Gantner. Are Bitcoin bubbles predictable? Combining a generalized Metcalfe’s Law and the Log-Periodic Power Law Singularity model. *Royal Society Open Science*, 6(6):180538, 2019. doi: 10.1098/rsos.180538.

A AI use disclosure

AI tools were used as research assistants throughout this work.

As research assistant. Claude Opus 4.7 (Anthropic) was used interactively throughout the research process to assist with: implementing the bootstrap, walk-forward, and figure-generation scripts; running the $K = 3$ wave-stability bootstraps across resolutions and series; fetching and integrating the additional cross-asset data; drafting text that documents the experiments; help revising the manuscript; and verifying internal consistency across sections. All scientific decisions were made by the human authors.

Manuscript review. Draft versions of the manuscript were reviewed using ChatGPT (OpenAI) in a simulated reviewer role, providing feedback on overclaiming, methodological gaps, and presentation issues. Several revisions — including the addition of standard forecasting baselines (RW-drift, auto-ARIMA, ETS, local-linear-trend), the specification-robust framing of the shift-sensitivity result, the bias–variance interpretation of the fit-prediction tradeoff, and the disclosure of selected auto-ARIMA orders — were motivated by this feedback.

Code verification. The same Claude Opus 4.7 assistant was used to audit the replication codebase for consistency between the manuscript and the analysis scripts, identifying and correcting several issues (stale on-chain data paths, cross-asset symbol mismatches, hard-coded values in figure scripts).

Authorship. In accordance with ICMJE guidelines,⁷ the human authors bear full responsibility for the integrity of the research, the correctness of the results, and the content of the manuscript. AI tools were used as assistants and do not meet the criteria for authorship. All outputs generated by AI — including code, text, and analytical suggestions — were reviewed, verified, and approved by the authors before inclusion.

⁷<https://www.icmje.org/recommendations/>